minerals

MDPI

Article

Handheld LIBS for Li Exploration: An Example from the Carolina Tin-Spodumene Belt, USA

Michael A. Wise [1], Russell S. Harmon [2,*], Adam Curry [2], Morgan Jennings [3], Zach Grimac [4] and Daria Khashchevskaya [2]

[1] Department of Mineral Sciences, National Museum of Natural History, Smithsonian Institution, Washington, DC 20560, USA; wisem@si.edu
[2] Department of Marine, Earth and Atmospheric Sciences, North Carolina State University, Raleigh, NC 27695, USA; accurry3@ncsu.edu (A.C.); dkhashc@ncsu.edu (D.K.)
[3] SciAps, Inc., 7 Constitution Way, Woburn, MA 01801, USA; mjennings@sciaps.com
[4] Piedmont Lithium, Inc., 5706 Dallas Cherryville Highway, Bessemer City, NC 28016, USA; zgrimac@piedmontlithium.com
* Correspondence: rsharmon@ncsu.edu; Tel.: +1-919-588-0613

Abstract: Laser-induced breakdown spectroscopy (LIBS), which has recently emerged as tool for geochemical analysis outside the traditional laboratory setting, is an ideal tool for Li exploration because it is the only technique that can measure Li in minerals, rocks, soils, and brines in-situ in the field. In addition to being used in many products essential to modern life, Li is a necessary element for a reduced carbon future and Li–Cs–Ta (LCT) granitic pegmatites are an important source of Li. Such pegmatites can have varying degrees of enrichment in Li, Rb, Cs, Be, Sn, Ga, Ta>Nb, B, P, and F. We focus here on the LCT pegmatites of the Carolina Tin-Spodumene Belt (CTSB) situated in the Kings Mountain Shear Zone, which extends from South Carolina into North Carolina. The CTSB hosts both barren and fertile pegmatites, with Li-enriched pegmatites containing spodumene, K-feldspar, albite, quartz, muscovite, and beryl. We illustrate how handheld LIBS analysis can be used for real-time Li analysis in the field at a historically important CTSB pegmatite locality in Gaston County, N.C. in four contexts: (i) elemental detection and identification; (ii) microchemical mapping; (iii) depth profiling; and (iv) elemental quantitative analysis. Finally, as an example of a practical exploration application, we describe how handheld LIBS can be used to measure K/Rb ratios and Li contents of muscovite and rapidly determine the degree of pegmatite fractionation. This study demonstrates the potential of handheld LIBS to drastically reduce the time necessary to acquire geochemical data relevant to acquiring compositional information for pegmatites during a Li pegmatite exploration program.

Keywords: laser-induced breakdown spectroscopy; LIBS; Li analysis; LCT pegmatites; K/Rb-Li systematics

Citation: Wise, M.A.; Harmon, R.S.; Curry, A.; Jennings, M.; Grimac, Z.; Khashchevskaya, D. Handheld LIBS for Li Exploration: An Example from the Carolina Tin-Spodumene Belt, USA. *Minerals* **2022**, *12*, 77. https://doi.org/10.3390/min12010077

Academic Editor: Paul Alexandre

Received: 30 November 2021
Accepted: 4 January 2022
Published: 9 January 2022

1. Introduction

Lithium is a metal widely used in the production of pharmaceuticals, glass, lubricants, and alloys; is present in most modern electronic devices; and used in many chemical processing and manufacturing processes [1]. It is also a critical element in the transition towards a low-carbon economy because it is central to the manufacture of the batteries that comprise energy storage systems and power electric vehicles. Because Li does not occur naturally as a native element, its current production comes from natural brines and granite-associated pegmatites in which Li concentrations have been strongly elevated above the average crustal abundance of 35 ± 11 ppm [2] to economically extractable levels. Brine deposits are the predominant source for Li at present (66%) and comprise the largest reserves but such deposits are geographically limited in distribution and face multiple production challenges. Pegmatite deposits (26%) will, therefore, remain an important source of Li because they are widespread globally and have a higher lithium concentration

compared to brines and clays [3–6]. Granitic pegmatites, in which Li typically occurs as a primary constituent in spodumene, petalite, and lepidolite, as well an important source of other important metals, including Be, Sc, Rb, Nb, Sn, Cs, Ta, REEs, Th, and U [7]. A particularly important type of granitic pegmatites is the Li–Cs–Ta (LCT) family [8,9].

2. Overview of LCT Granitic Pegmatites

LCT pegmatites are largely considered to be late magmatic products of extreme fractionation of peraluminous S-type granites [8], although the anatectic melting of supracrustal and mantle-related source lithologies has been proposed as an alternative process for the generation of some LCT pegmatite populations [10–12]. Granites parental to LCT pegmatites (i.e., fertile granites) often occur as texturally heterogeneous, zoned plutons that may include facies of (i) fine-grained biotite granite, (ii) two-mica granites, (iii) coarse-grained pegmatitic leucogranites, (iv) sodic aplites; and (v) highly mineralized pods and lenses of pegmatites in the apical portions of the pluton [13].

The population of LCT pegmatites cogenetic with fertile S-type granites ranges from barren bodies that lack significant rare-element mineralization to pegmatites that display varying degrees of enrichment in Li, Rb, Cs, Be, Sn, Ga, Ta > Nb, B, P, and F. This moderate to extreme fractionation of pegmatite melts typically results in rare-element mineralization that includes beryl, columbite-group minerals, the compositionally complex borosilicate tourmaline, and Li-minerals, such as triphylite-lithiophilite, amblygonite-montebrasite, spodumene, petalite, and lepidolite.

In many districts and fields, granite-pegmatite suites show patterns of regional zoning where LCT pegmatites are situated within 10 km of their parental granite [14]. The exposed regional zoning pattern is rarely concentric, but instead is asymmetrical in most pegmatite fields and strongly influenced by the nature and structure of the host rock, by the shape of the parental intrusion, and the current erosional level of the granite–pegmatite system. In general, the least evolved and poorly mineralized bodies are found closest to the margins of the source granitic pluton, whereas the most chemically evolved Be-, Ta-, and Li-enriched pegmatites occur in distal areas relative to the parental pluton [15]. Spodumene- and petalite-bearing pegmatites typically occur the farthest away from their parental granite. This oversimplified sequence of pegmatite types extending outward from the margins of their parental granite is further characterized by progressive complexity of internal structural zones/units within individual pegmatite bodies, increasing diversity of mineral species, increasing degrees of metasomatic replacement, along with a gradual enrichment in Li, Rb, Cs, B, P, and F.

From an economic perspective, elemental abundance (e.g., Rb, Cs, Ta) and ratios (e.g., K/Rb, K/Cs, Nb/Ta) serve as valuable tools for the rapid assessment of the degree of rare-element fractionation in granite-pegmatite suites. Typically, low values of K/Rb (~2–400) and K/Cs (~20–2000) in K-feldspar, K/Rb (~1–50) and K/Cs (~10–1000) in muscovite, Na/Li (~2–20) in beryl, Fe/Mn in garnet (~0.007–2.0), Nb/Ta (~0.001–24) in columbite-group minerals, and Zr/Hf (~0.01–13) in zircon are encountered in pegmatites that have undergone moderate to extreme levels of fractionation and accumulation of rare lithophile elements [16,17]. These geochemical indicators of fractionation have been successfully used to identify parental granitoids, establish regional trends of rare-element enrichment in large pegmatite populations, and distinguish barren from mineralized pegmatites suitable for the extraction of potential rare-element ore minerals.

3. Geological Setting of the Carolina Tin-Spodumene Belt

The Carolina Tin-Spodumene Belt (CTSB) is of particular importance as a host of the most extensive and historically important Li pegmatite deposit in North America. Here, pegmatites of Carboniferous age [16] are concentrated in a belt across the Kings Mountain Shear Zone. This 0.5 to 3-km-wide, northeast-trending structure marks the boundary of the Inner Piedmont and Kings Mountain lithotectonic domains, with the shear zone extending approximately 60 km from Gaffney, South Carolina to Lincolnton, North Carolina (Figure 1).

Enclosed within the metamorphic rocks of the CTSB, which exhibit evidence of multiple periods of deformation, are hundreds of granitic pegmatite dikes, many containing spodumene and the tin oxide mineral cassiterite. Pegmatite intrusion occurred after major periods of deformation, but before the last of the tectonic movement [18,19]. The peraluminous 2-mica Cherryville granite lies just west of the CTSB in the Inner Piedmont belt and is considered by some investigators to be the source of the CTSB pegmatites, although derivation from the biotite-bearing High Shoals granite east of the CTSB has also been suggested [20–25].

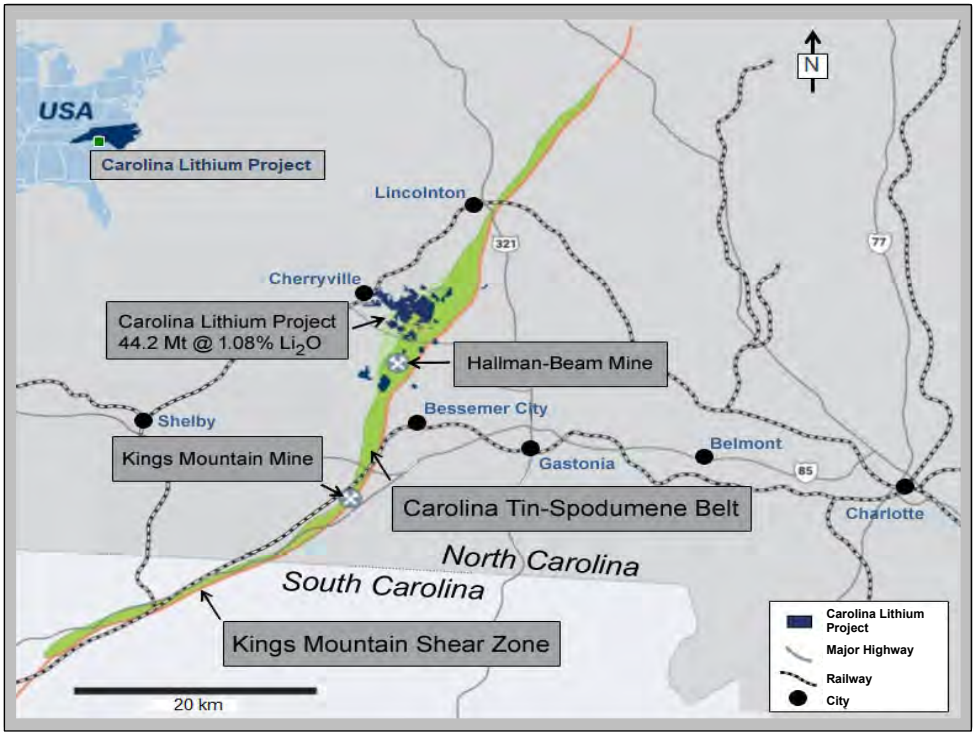

Figure 1. Carolina Tin-Spodumene Belt (green) showing the Kings Mountain Shear Zone (orange), the Kings Mountain and Hallman-Beam Li mines, and Piedmont Lithium's Carolina Lithium Project (CLP) prospect in Gaston County, N.C. that has an estimated reserve of 44.2 Mt at 1.08 wt. % Li_2O (modified from map provided by Piedmont Lithium Inc. on 29 October 2021).

Different types of pegmatites have been identified within the CTSB that include (i) barren pegmatites containing primarily K-feldspar, oligoclase, quartz, with accessory muscovite, biotite, and garnet; (ii) barren pegmatites composed of K-feldspar, albite, quartz, and beryl; and (iii) lithium pegmatites bearing spodumene, K-feldspar, albite, quartz, and beryl [26]. Barren granitic pegmatites are most common within and near the Cherryville granite, whereas spodumene-bearing pegmatites are concentrated away from the granite body [27]. Accessory minerals in the pegmatites include beryl, garnet, titanite, cassiterite, zircon, Mn-bearing fluorapatite, triphylite, and columbite-group minerals [28,29].

Individual Li-bearing pegmatites are complex structures having typical surface dimensions of a few to a hundred meters in width and up to a kilometer in length that were intruded generally parallel to foliation in the surrounding country rocks [21]. Typically having a modal composition of ~20% spodumene, ~32% quartz, ~41% feldspar, and ~6% muscovite (Figure 2), these pegmatites are remarkably homogeneous, with minimal internal compositional zoning [23,28]. As illustrated in Figure 3, CTSB pegmatites can be quite coarse grained, with individual crystals > 1 m in length.

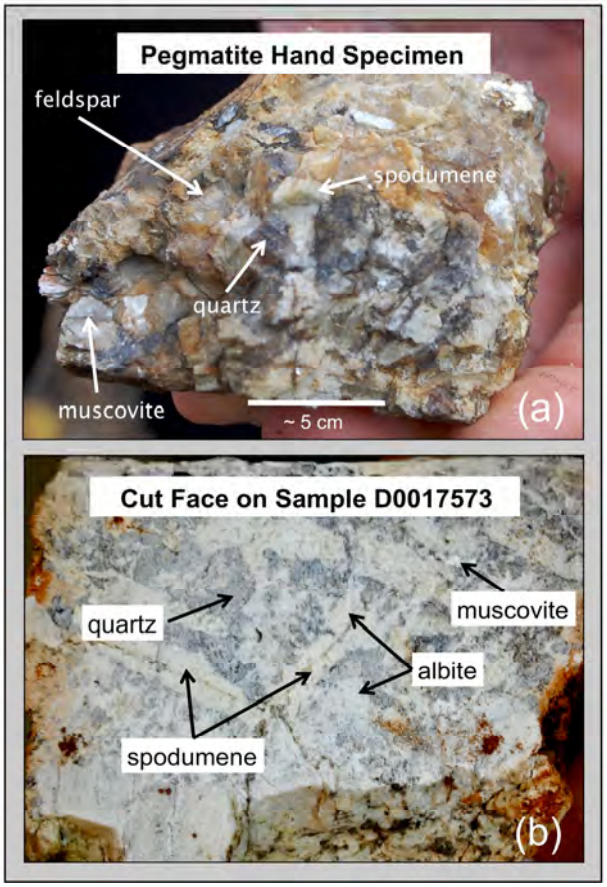

Figure 2. Two samples from the CLP in Gaston County, North Carolina: (**a**) hand specimen showing the typical mineralogy of spodumene, feldspar, quartz, and muscovite; (**b**) slab face of outcrop sample D0017573 showing a mineralogy of spodumene, quartz, albite, and muscovite.

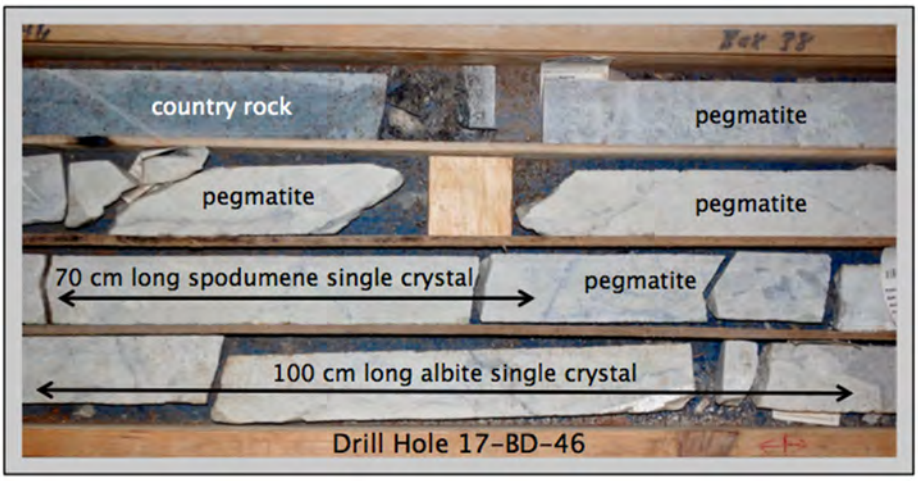

Figure 3. Carolina Lithium Project drill core 17-BD-46 between 107.51–110.21 m depth showing from top to bottom metamorphic country rock, and typical pegmatite containing a 70-cm-long crystal of spodumene and a 1-m-long albite crystal.

Estimates of Li reserves for the CTSB are large, >100 Mt averaging about 0.7% Li [30]. Active mining of spodumene was undertaken in the CTSB from the 1950s–1990s at two major mines: the Kings Mountain Mine operated by the Foote Mineral Company and the Hallman-Beam Mine operated by the Lithium Corporation of America (Figure 1). Recent

industrial demand for Li has resulted in renewed exploration activity across the CTSB, with the Piedmont Lithium's Carolina Lithium Project (CLP) presently assessing a large prospect in Gaston County near Bessemer City (Figure 1). The in-field LIBS analyses reported here were undertaken on drill core and at multiple outcrops across this prospect.

4. Laser-Induced Breakdown Spectroscopy

Laser-induced breakdown spectroscopy (LIBS) is a versatile form of atomic emission spectroscopy that can be used qualitatively for elemental detection or quantitatively for determination of elemental concentration [31,32] and references therein. In LIBS, a rapidly pulsed laser beam is focused onto a sample to ablate a minute amount of it and create a plasma on the sample surface in which constituent elements can be detected and identified through spectral analysis of emitted light. Because all elements have at least one emission line over the spectral range between 200–900 nm, any element can be analyzed by LIBS in situations where its abundance is above the limit of detection in the materials of interest [32]. As discussed by Harmon and Senesi [31], the rapid acquisition by LIBS of such information can be particularly useful to the mining industry for resource exploration and grade control during mining and ore beneficiation.

LIBS was one of many techniques restricted to chemical analysis in the laboratory or in industrial settings that have included mine and ore-processing sites [33] until the introduction of commercial handheld LIBS analyzers in 2016 [34]. Since that time, handheld LIBS has been used for a variety of geological applications that include the identification of elements and minerals; the discrimination of carbonate muds, limestone/dolomite stratigraphic sequences, volcanic rock suites, and meteorites; and natural resources exploration [35–49]. An important governing consideration with LIBS is the set of chemical and physical phenomena termed 'matrix effects' e.g., [31,50] and references therein, which determine the amount of mass ablated by an incident laser pulse. Chemical matrix effects occur when the emission behavior of one element in the plasma is interfered with by the presence of another element. By contrast, physical matrix effects arise from the nature of the sample. For example, there are a multiplicity of factors that determine the extent of laser–material coupling with geological materials, and therefore the resultant plasma character, which is primarily determined by the nature of the sample (e.g., its compositional homogeneity, degree of crystallinity or induration, hardness, grain size and porosity, surface texture and roughness, moisture and organic content, absorptivity and thermal conductivity, and optical transmissibility and reflectivity). Although full, broadband LIBS spectra may be used without preprocessing for elemental detection and applications, such as geochemical fingerprinting [50], the shot-to-shot variation that characterizes LIBS analysis of geological materials requires preprocessing that includes baseline correction of spectra and peak intensity normalization for development of calibration curves for quantitative analysis [51–55].

4.1. Laboratory LIBS Analysis of Li in Geological Materials

Li is an element effectively analyzed by LIBS because of its strong emissivity, which makes it readily detectable in geological materials, even when present at low ppm abundance levels. Analysis of Li in geological materials has been demonstrated in several studies over the past two decades using laboratory LIBS systems.

Fabre et al. [56] developed a quantitative calibration using 16 synthetic glasses and two micas that had a detection limit for Li of ~0.0005 wt. %. This calibration was then used to estimate the Li content of a suite of Li-bearing minerals that included spodumene and petalite with 6–8 wt. % Li from granite-associated pegmatites in Portugal, the glass (0.009–0.044 wt. %), and daughter minerals (up to 6.2 wt. % Li) for melt inclusions in quartz phenocrysts in a rhyolite from the Streltsovka caldera in the Transbaikalia region of eastern Russia, and in hydrothermal and diagenetic quartz (up to 0.034 wt. %) from the Sierra de Guadarrama in central Spain. McMillan et al. [57] observed strong Li emission in a LIBS survey of more than 96 beryls from 16 countries, and McManus et al. [58] determined that

Li was an important element for discriminating the provenance of beryl from pegmatite locations across the New England region of the northeastern United States.

Sweetapple and Tassios [59] demonstrated semi-quantitative mapping of Li, Be, and B in altered spodumenes and other Li-rich minerals from the Neoarchean Mt. Cattlin Li-pegmatite deposit in Australia and used this to discriminate spodumene; its accompanying sericitic alteration; and the matrix minerals, lepidolite, albite, and quartz. This study estimated a Li detection limit of ~0.024 wt. % based on Li-doped borosilicate glass as standards.

LIBS microchemical mapping and chemometric analysis was utilized by Romppanen et al. [60] to identify and discriminate the Li-bearing ore mineral spodumene from gangue minerals across the Kaustinen LCT pegmatite province of western Finland and to map sample texture. That same year, Janovszky et al. [61] undertook LIBS analysis of monzogranite from the Mórágy Granite Complex in the Eastern Mecsek Mountains of Hungary for the classification of constituent mineral grains and for Be and Li prospecting in granitoid rocks. This study demonstrated that valuable information about the distribution of elements in minerals can be obtained from LIBS elemental mapping, especially when combined with emission intensity data derived from matrix-matched calibrations.

Riberio et al. [62] used a portable XRF analyzer and a bespoke laboratory LIBS system to examine the same locations on quartz, montebrasite, and turquoise in a slab cut from a hydrothermal vein at the Argemela Tin Mine in Central Portugal. LIBS results demonstrated that montebrasite can be distinguished from turquoise because the turquoise did not contain Li. Micromapping by LIBS was successful in identifying minerals and their alteration products in a petrographically described thin section. The differences in spot size between XRF (5 mm) and LIBS (300 μm) resulted in a poorer performance by XRF in accurately identifying mixed minerals.

4.2. Li Analysis by Handheld LIBS

Senesi [39] described the potential for handheld LIBS analysis across the geosciences. Subsequently, Harmon et al. [37] described the use of a SciAps Z-300 handheld LIBS analyzer for quantitative Li analysis on-site during an exploration campaign at the Agua Fria Li prospect in the Sonora region of Mexico, where a Li-bearing hectorite clay and marl sequence is contained within the clastic sediments of an Oligocene to Miocene volcano-sedimentary basin sequence. The multielement composition of composite samples from 3 m intervals of the drill core was determined by ICP-MS analysis. LIBS measurements taking <3 seconds each to acquire for a 3 × 4 raster pattern at 12 locations on pressed pellets of each composite sample were averaged to produce a single-composite LIBS spectrum. The Li contents determined by handheld LIBS analysis agreed well with the laboratory results, with an R^2 observed of 0.86 for the suite of core samples analyzed.

Most recently, Fabre et al. [63] described the use of a SciAps Z-300 handheld LIBS instrument in the laboratory to acquire >4000 LIBS spectra for the Li-bearing minerals, including spodumene, petalite, lepidolite, zinnwaldite, amblygonite, or montebrasite, as well as various altered Li minerals and pegmatite samples from the Fregenda–Almendra pegmatite field that outcrops from the Guarda district in Portugal to the Salamanca province in Spain. These analyses were undertaken on minerals, rock thin sections, and pressed powder pellets and glasses prepared from pulverized minerals. The major elements observed were Al, Si, O, Mg, Ca, Li, Na, K, and Fe, with Be, Sr, Ba, Cs, Sn, Ta, and W being the most common minor and trace elements identified.

5. Analytical Methodology and Samples

Handheld LIBS is an attractive tool for undertaking geochemical measurements during exploration, drilling, or ore assessment campaigns because in-situ analytical results can be acquired rapidly under ambient environmental conditions with a minimum of sample preparation. Handheld LIBS analyzer has a unique capability to answer three questions in the field for the exploration geologist:

- What elements are present in a mineral, rock, or soil?
- How much of an element of interest is present?
- Is a sample compositionally homogeneous?

5.1. Samples

A wide variety of samples from the CLP prospect (Figure 1) were analyzed on site during 21–22 October 2021, either at the core storage facility (Figure 3) or at field outcrops (Figure 4) that included minerals in the drill core and outcrop, the pulverized drill core, and the soil. Minerals analyzed included spodumene, muscovite, quartz, albite, K-feldspar, tourmaline, and vivianite.

Figure 4. In-field LIBS analysis of pegmatite outcrops on the Carolina Lithium Project prospect in Gaston County, N.C., showing the use of the handheld LIBS analyzer for in-situ analysis (**a**) and examples of the different minerals analyzed—feldspar (**b**); feldspar, quartz, spodumene, and tourmaline (**c**); spodumene (**d**); and quartz (**e**).

5.2. Handheld LIBS Analysis

For this study, we used a SciAps Z-300 handheld LIBS analyzer (Figure 4). This instrument contains a Nd:YAG diode-pumped solid-state pulsed laser that generates a beam of focused laser light at 1064 nm that delivers a 5–6 mJ pulse of 1 ns pulse duration onto a 100-μm area of the sample at a user-selected firing rate between 1 and 50 Hz. The instrument records light emission from the LIBS plasma, typically after a 650 ns delay over a 1-ms integration time, between the 190 to 950-nm spectral range, over which every element has at least one emission line. The Z-300 has the capability for the analysis to be conducted in Ar, which confines the plasma for enhanced emission, particularly in the deep ultraviolet portion of the LIBS emission between 190–300 nm. The light signal is collected and passed by fiber optic cable into three spectrometers with time-gated, charge-coupled

diode (CCD) detectors having respective spectral ranges and resolutions of 190–365 nm with a full-width half-maximum (FWHM) value of 0.18 nm, 365–620 nm with a FWHM value of 0.24 nm, and 620–950 nm with a FWHM value of 0.35 nm. This analysis produces composite LIBS spectra over the 23,432 channels of the spectrometer.

The sections that follow present examples of the *Element Pro, Geochem, and Geochem Pro* applications that are the on-board software programs facilitating the broad analytical capability of the Z-300 analyzer. Before our fieldwork, calibrations were prepared on the instrument in the laboratory for mica and bulk powdered pegmatite of known composition prior to using it at the CLP prospect to answer the three questions posed above. Four different analytical approaches were employed. First, for elemental identification using the *Element Pro* application, averages of four recorded spectra were collected after two cleaning shots at a laser firing rate of 50 Hz across a 4 × 3 grid. Next, microscale mapping with the *Geochem Pro* application was undertaken with a single laser shot at 256 locations over a 16 × 16 grid over 2 mm^2 areas of mineral surfaces to obtain distributions of elemental relative concentrations in the form of relative abundance 'heat maps'. Then, elemental depth profiles were obtained by firing between 288-300 successive laser shots at single locations and recording 4-shot averages. Finally, quantitative analysis for Li was undertaken using the *Geochem* application by processing the average LIBS intensity values obtained from averaging of four spectra from 12 locations on a sample using the on-board calibrations.

The sections that follow present examples of the *Element Pro, Geochem, and Geochem Pro* applications described above. Before our fieldwork, calibrations were prepared on the Z-300 in the laboratory for mica- and bulk-powdered pegmatite of known composition, prior to using the handheld LIBS instrument at the CLP prospect to demonstrate its capability to answer the three questions posed above. Four different analytical approaches were employed, all of which used the option to undertake the LIBS analysis in an Ar atmosphere. First, for elemental identification using the *Element Pro* application, averages of four recorded spectra were collected after two cleaning shots at a laser firing rate of 50 Hz across a 4 × 3 grid. Next, microscale mapping with the *Geochem Pro* application was undertaken with a single laser shot at 256 locations over a 16 × 16 grid over 2 mm^2 areas of mineral surfaces to obtain distributions of elemental relative concentrations in the form of 'heat maps'. Then, elemental depth profiles were obtained by firing between 288–300 successive laser shots at single locations and recording 4-shot averages. Finally, quantitative analysis for selected elements was undertaken using the *Geochem* application by processing the average LIBS intensity values obtained from averaging of four spectra from 12 locations on a sample using the calibration.

6. Application, Results, and Discussion

Exploration programs for rare-element granitic pegmatites typically utilize an integrated geological, mineralogical, and geochemical approach for identifying exposed and buried pegmatites of economic interest. Rock and mineral geochemistry has proven to be extremely effective in differentiating barren pegmatites lacking rare-element minerals from pegmatites that carry significant Be, Nb, Ta, Sn, or Li mineralization. The trace element content of pegmatite feldspars and micas have been proven to be useful markers for distinguishing chemically primitive pegmatites from moderately to highly evolved rare-element enriched pegmatites [16]. In a pegmatite field or district, where tens to hundreds of mineralogically diverse pegmatite bodies may be present, the inexpensive and rapid analysis of Li, K, Rb, and Cs in feldspar and muscovite by handheld LIBS can be a unique tool for identifying prospective Li-enriched pegmatites in the field during an exploration program.

The wallrock of some LCT pegmatites may develop exomorphic halos enriched in Li, Rb, Cs, B, and Be via interaction with pegmatite-derived fluids [64,65]. The occurrence of exomorphic minerals, such as holmquistite, biotite, tourmaline, and emerald, in amphibolitic and schistose wallrock surrounding pegmatites attest to episodes of metasomatic alteration, which have been shown in some cases to be a useful tool in pegmatite exploration. LIBS analysis of alteration assemblages in wallrocks surrounding rare-element-enriched peg-

matites has the potential to be an integral part of any pegmatite exploration program aimed at targeting Li-enriched pegmatites.

The geochemistry of soils and saprolite overlying pegmatite bodies has been shown to be successful in finding buried rare-element pegmatites [66]. Soils and saprolites that develop from weathered pegmatites can maintain low levels of trace elements inherent to the unweathered pegmatite body [67,68]. Because LIBS instruments can quickly detect low levels of Li and other trace elements, handheld LIBS is ideally suited for conducting soil surveys in pegmatite fields where outcropping bodies are scarce or absent.

6.1. Elemental Detection

For rapid qualitative analysis, the Z-300 is used in the *Element Pro* mode for element detection and identification. Relative emission strengths for each emission line in an acquired broadband LIBS spectrum are interrogated and compared with an onboard spectral library of selected elemental emission lines for the entire periodic table derived from the NIST atomic spectra database [69]. After each analysis, the list of elements identified in the sample is displayed (Figure 5), accompanied by a "likelihood" ranking that is a measure of the ratio of the number of elemental emission lines present in an acquired spectrum to the number of lines for each element in the spectral library and an estimated elemental "relative abundance" comparing how much of an element is present in the sample compared to other elements, with the caveat that there is no direct correlation between relative abundance and absolute element concentration. Used in this way, handheld LIBS analysis can be employed in the field to (i) detect the main elements present in a rock, mineral, or soil; (ii) rapidly distinguish between minerals of similar appearance; or (iii) identify an unknown mineral.

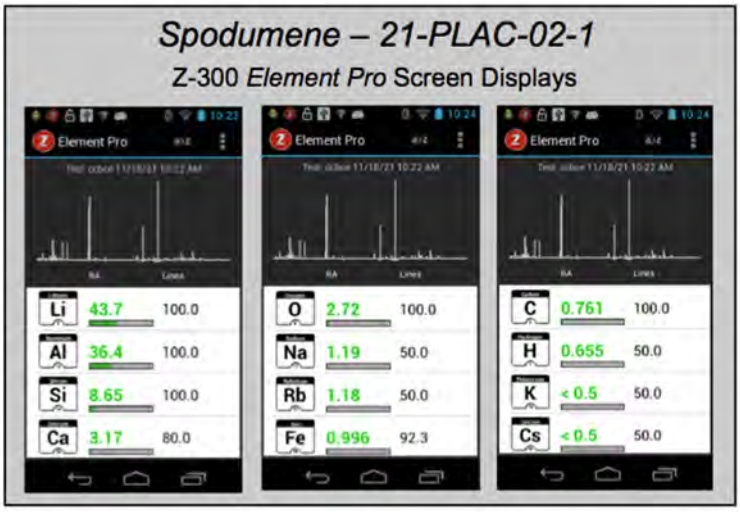

Figure 5. Z-300 screen shot sequence generated at the time of analysis showing the LIBS spectrum for spodumene in pegmatite outcrop 21-PLAC-02 on the Carolina Lithium Project prospect in Gaston County, N.C. and the 12 elements recognized with confidence in this sample—Li, Al, Si, Ca, O, Na, Rb, Fe, C, H, K, and Cs. The number in black text on the right-side column is the "likelihood" value, i.e., percentage of spectral lines in the on-board spectral library present in the LIBS spectrum, whereas the green number in the middle column is the "relative abundance" value. See text for discussion.

Analysis using the Z-300 handheld LIBS instrument identified 20 elements present in minerals of the pegmatite rock samples, drill cores, and outcrops analyzed across the CLP prospect above their different limits of detection (Table 1)—Al, B, Ba, Be, Ca, Cs, Fe, H, K, La, Li, Mg, Mn, Na, O, P, Rb, Si, Sr, and V in some samples. Most elements are observed in the primary pegmatite minerals spodumene, quartz, feldspar, and/or muscovite; H and O are most pronounced in hydroxyl-bearing species; Be and La are only observed in the aluminosilicates; and P is only present in the phosphates (Figures 6–9). This is essentially

the same set of elements recorded by Fabre et al. [63] in their handheld LIBS analysis of Li-bearing pegmatite minerals from the Fregenda–Almendra pegmatite field of the Iberian Peninsula.

Table 1. Emission lines for most common elements identified in pegmatite minerals from the Carolina Lithium Project prospect in Gaston County, North Carolina (USA).

Element	Wavelength (nm)	Wavelength (nm)	Wavelength (nm)	Element	Wavelength (nm)	Wavelength (nm)	Wavelength (nm)
Al	394.40	396.15	309.77	Li	670.79	610.36	460.29
B	249.77	249.68	-	Mg	279.53	282.27	285.22
Ba	455.40	553.55	493.41	Mn	257.61	260.57	356.95
Be	313.04	-	-	Na	589.00	589.59	-
Ca	393.37	396.85	422.67	O	777.20	-	-
Cs	852.11	894.35	257.80	P	213.62	214.95	-
Fe	259.94	438.35	371.99	Rb	780.03	794.76	-
H	656.28	-	-	Si	288.16	251.61	390.55
K	766.49	766.90	404.41	Sr	407.78	460.73	-
La	492.18	518.34	505.65	V	267.93	373.73	410.98

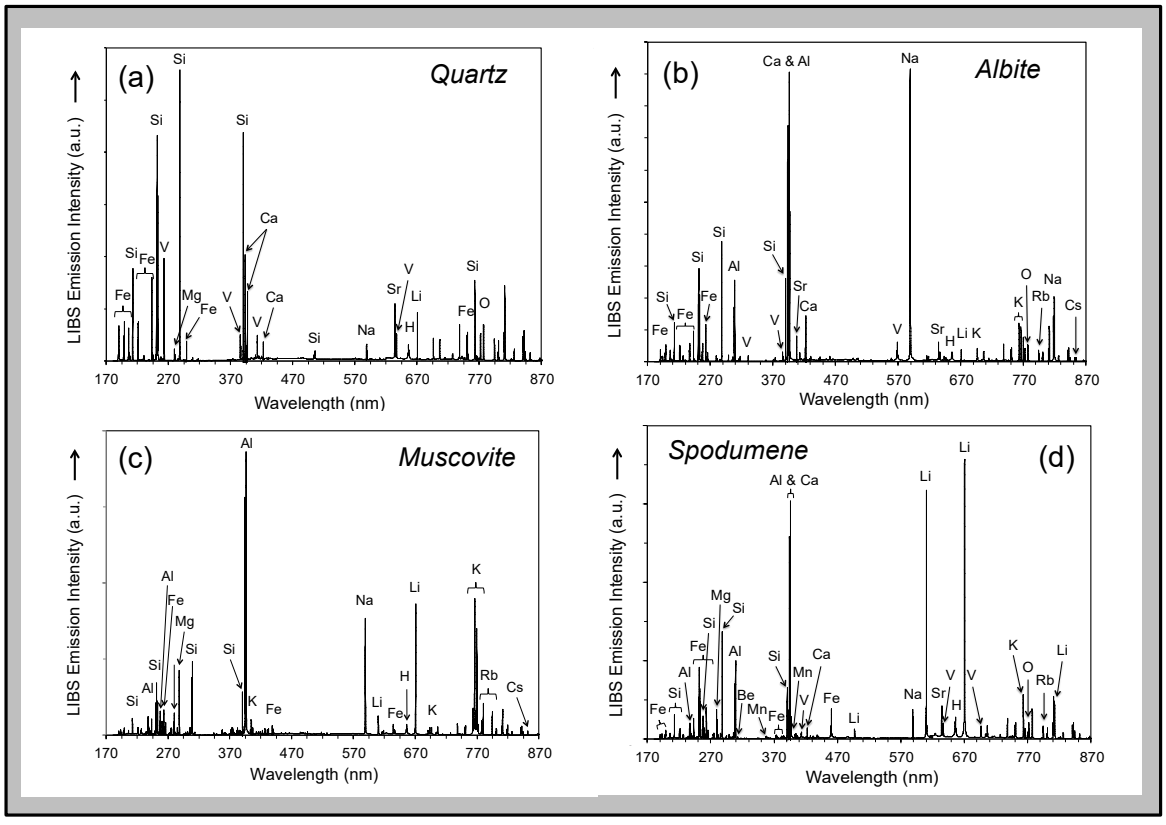

Figure 6. Handheld LIBS spectra for the primary pegmatite minerals quartz (**a**), albite (**b**), muscovite (**c**), and spodumene (**d**) from pegmatite outcrops on the Carolina Lithium Prroject prospect in Gaston County, N.C. The unlabeled peaks in the infrared portion of the spectrum between 700–870 nm are for the Ar purge gas used for the analysis.

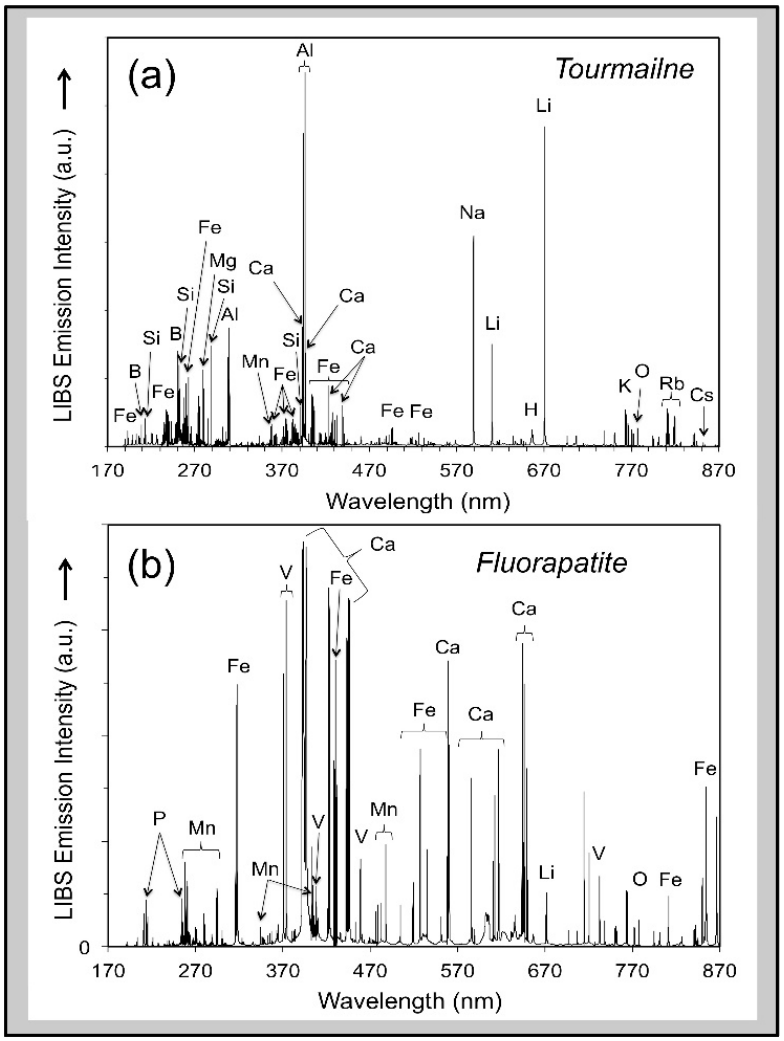

Figure 7. Handheld LIBS spectra between 170–870 nm for the pegmatite accessory minerals tourmaline (**a**) and fluorapatite (**b**) in pegmatite samples from the Carolina Lithium Project prospect in Gaston County, NC. The unlabeled peaks in the infrared portion of the spectrum between 700–870 nm are for the Ar purge gas used for the analysis.

Visually distinguishing between feldspar and spodumene or the micas muscovite and lepidolite rapidly in outcrops during an exploration campaign can sometimes be difficult but is immediately obvious by comparison of LIBS spectra based on the presence of the primary Li emission peaks at 610.36 nm and 670.79 nm in the Li-rich minerals (Figure 6). Similarly, phosphate minerals can be readily identified because the Z-300 analyzer records the ultraviolet region of the LIBS emission spectrum and, therefore, can observe the P emission lines at 213.62 nm and 214.95 nm (Figure 7). Non-metal elements, such as F, are particularly difficult to analyze by spectroscopic techniques, so it is notable that the two prominent molecular bands for CaF between 529–543 nm and 590–606 nm are present in the LIBS spectra for tourmaline and fluorapatite shown in Figure 7. Residual minerals in the regolith cover of the critical zone can be a useful guide to the presence of mineralized pegmatite at depth. For example, the presence of Li in detrital quartz in areas of deep soil cover lacking outcrop can be an important pathfinder to mineralization in the subsurface. Finally, under favorable circumstances, LIBS analysis can be helpful for rapid identification of accessory and uncommon minerals can be readily identified on site through a LIBS analysis (Figure 7).

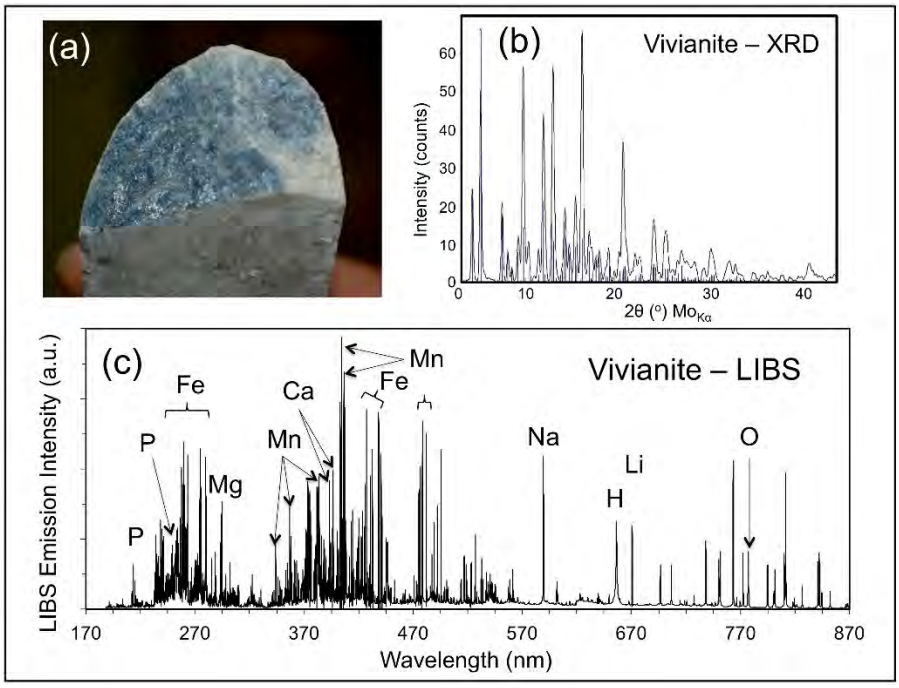

Figure 8. (**a**) Fine-grained vivianite [$Fe_3(PO_4)_2 \cdot 8H_2O$] on a fracture in drill core 18-BD-288 from the Carolina Lithium Project prospect in Gaston County, N.C.; (**b**) X-ray diffraction pattern (Mo Kα radiation) of vivianite after background subtraction (black), with International Centre for Diffraction Data pattern matches shown by vertical blue bars; and (**c**) handheld LIBS spectrum of vivianite showing the prominent P peaks at 213.62, 214.92, and 255.32 nm and the major Li peak at 670.79 nm. The suite of weak unlabeled peaks in the ultraviolet and visible portions of the LIBS spectrum between 234–278 nm and 404–441 nm are Fe emissions. The unlabeled peaks in the infrared portion of the LIBS spectrum between 700–870 nm are for the Ar purge gas used for the LIBS analysis. The very strong H peak at 656.3 nm in this spectrum, compared to those shown in Figures 6 and 7, indicate that this sample is a hydrated mineral and further supports its identification as vivianite.

Late-stage mineralization is common along fissures and fractures throughout the strongly tectonized and deformed CTSB. Figure 8 shows the occurrence of a blue-black, hypidiomorphic mineral along a fracture plane in a drill core (a) that was analyzed by X-ray diffraction analysis (b), and LIBS (c). LIBS analysis identified the presence of Fe, Li, and P, indicating that this mineral was either triphylite [$LiFePO_4$] or vivianite [$Fe_3(PO_4)_2 \cdot 8H_2O$] produced from the alteration of triphylite, with the latter attribution subsequently confirmed by the X-ray diffraction analysis.

6.2. Element Spatial Distribution

Whole-rock lithogeochemistry of outcrop and drill core samples, together with microscale analysis of individual minerals, are two of the primary exploration tools for mapping the geochemical signature of ore systems. LIBS can be helpful in this context in two different ways. The Z-300 analyzer has a computer-controlled 3-D translational stage that permits rastering of the laser beam across the sample in the XY-direction at 12.5 μm steps over an area of up to 2 × 2 mm^2, with the grid size and the number of laser shots fired at each point defined by the user. A user-selected number of non-analytical 'cleaning' shots can be performed prior to data collection. Therefore, compositional variation within a sample can be examined by the Z-300 analyzer at the ~100 μm spatial scale of the LIBS analysis through either the microscale mapping feature where the laser is rastered over a 2 mm area of the sample surface or by depth profiling in which successive laser shots are undertaken at the same spot to ablate a sample to progressively greater depths.

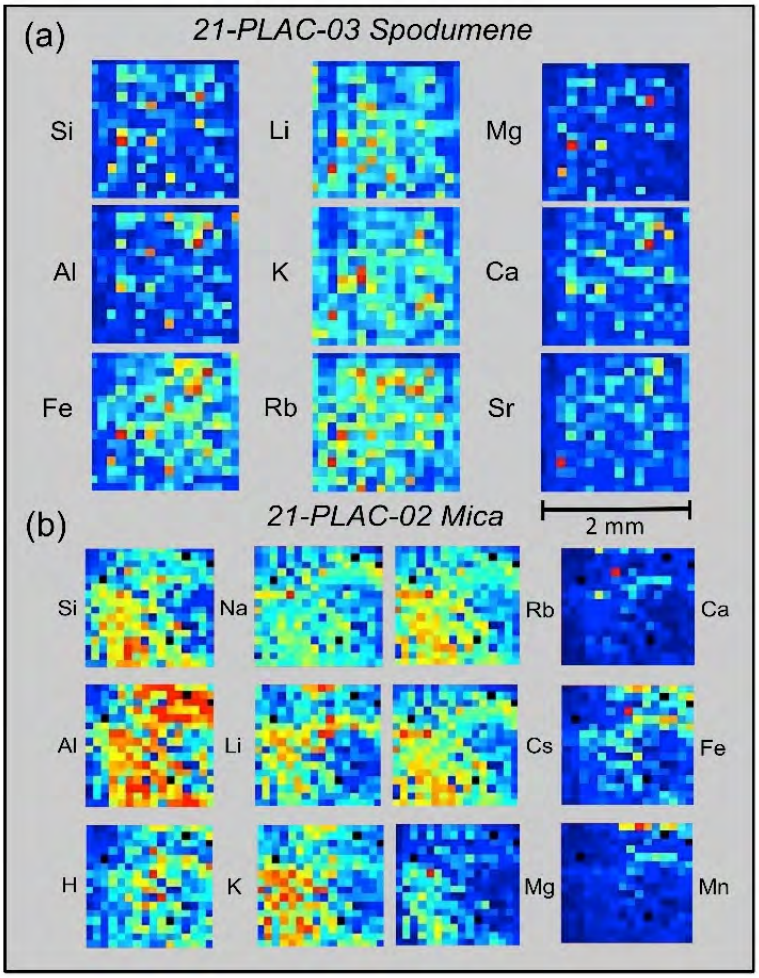

Figure 9. Elemental distribution 'heat maps' obtained by Z-300 raster scanning of a spodumene (**a**) and muscovite (**b**) specimens from outcrops on the Carolina Lithium Project prospect in Gaston County, N.C. Elemental emission intensity variations for different elements are shown in a gradient of colors that varies from red for high relative abundance to blue for low relative abundance. The spectral lines used for these microchemical maps are: Al = 396.15 nm, Ca = 393.37 nm, Cs = 852.11 nm, Fe = 438.35 nm, H = 656.28 nm. K = 766.49 nm, Li = 670.79 nm, Mg = 279.55 nm, Mn = 403.31 nm, Na = 588.99 nm, and Si = 288.16 nm.

For microscale mapping, the *Geochem Pro* mode of the Z-300 analyzer is used to identify spectral peaks and then generate relative concentration maps based on the recorded elemental intensities [37,46]. 2-D maps of relative emission intensity, commonly termed 'heat maps', are produced from individual laser shots spaced 12.5 µm across the surface of a sample over a 16 × 16 grid pattern. Examples from the CLP prospect are shown in Figure 9 for spodumene and muscovite crystals from two outcrop samples, 21-PLAC-03 and 21-PLAC-02. Such information can reveal whether a mineral is homogeneous at the spatial scale of the LIBS analysis and also can be helpful in understanding the geochemical behavior of different elements at a small spatial scale, which can provide insight into the process of pegmatite formation.

The panels in Figure 9a display the spatial distributions of variations in Si, Al, Fe, Li, K, Rb, Ca, Mg, and Sr abundances on the surface of a spodumene crystal in outcrop sample 21-PLAC-03, whereas those in Figure 9b show the spatial distributions of variations in Si, Al, H, Na, Li, K, Rb, Cs, Ca, Fe, and Mn abundances across a 2-mm domain on the surface of a muscovite crystal in outcrop sample 21-PLAC-02. Two features are of particular note across the 2 × 2 mm^2 surface domains for the element distributions shown in Figure 9. The first is the general compositional homogeneity of the spodumene compared to the muscovite at

this spatial scale. By comparison to the nine 'heat maps' for 21-PLAC-03 spodumene, which are dominated by shades of dark and light blue, the individual 'heat maps' for 21-PLAC-02 muscovite exhibit the full range of color variation from almost entirely dark blue for Ca and Mn to domination by yellow and red colors for Al. The second is the coherent geochemical behavior of Li-K-Rb and Mg-Ca-Sr for the spodumene and Li-Na-K-Rb-Cs and Ca-Fe-Mn for the muscovite.

Figure 10 shows depth profiles for spodumenes in two outcrops. The profiles represent 4-shot averages of LIBS emission intensities of 10 spectral lines ($Mg_{279.52}$, $Si_{288.16}$, $Be_{313.04}$, $Al_{309.27}$, $Ca_{422.67}$, $Na_{589.59}$, $Li_{610.36}$, $K_{766.49}$, $Rb_{794.76}$, and $Cs_{852.11}$) for 300 successive laser shots at a single spot on sample 21-PLAC-03 and 288 successive laser shots at a single spot on sample 21-PLAC-04. These intensity variations are displayed on a logarithmic scale, as element intensities vary over five orders of magnitude for sample 21-PLAC-03 and four orders of magnitude for sample 21-PLAC-04. Thus, elements present in the samples at high abundance show subdued variation compared to elements of low concentration. Both depth profiles are characterized by significant variation over the first 5–6 depth intervals (i.e., 20–24 laser shots), which records decreases for some elements (e.g., Na, Mg, Ca) yet increases for others (e.g., Si, Al, Li, Rb, Cs). This behavior is interpreted to reflect the cumulative effect of surficial weathering of the spodumene that has caused elements of contrasting geochemical behavior being mobile to different extents. The other feature of note is the sharp increases in emission intensity for Na, Mg, Ca, K, and Be together with concomitant intensity decreases for Si, Al, Rb, and Cs observed for spodumene 21-PLAC-04 over the 40–45 laser shot depth interval. This compositional discontinuity likely reflects the encounter of the laser beam with an inclusion a few 10s of microns in size. Fabre et al. [56] have described how such inclusions can be probed and compositionally interrogated using a laboratory LIBS system.

6.3. Quantification

LIBS can measure the elemental abundance by measuring the intensity of the light captured at specific spectral wavelengths because the intensity of the plasma emission is proportional to the concentration of an element in a material of interest. Quantitative analysis by LIBS can be straightforward if the material being analyzed is compositionally homogeneous, as is the general situation for metal and alloy analysis where LIBS is well established and has been widely applied for a variety of industrial applications [33,40,70–75]. This is not generally the case for geological materials, which are intrinsically variable in terms of composition, crystallinity, and texture. Both the chemical composition of the matrix being analyzed by LIBS and its physical characteristics affect the measured abundance of an analyte present in the plasma [32] because these characteristics directly influence the excitation properties of the laser plasma produced by the ablation process [76] and, therefore, the emission line intensity measured for any element. Chemical matrix effects arise when the presence of an element of low ionization potential in the plasma elevates the plasma density and thereby inhibits the emission of other elements to decrease their abundance in the plasma [77]. Differences in material physical characteristics, such as crystallinity, hardness, opacity, grain size, coherence and texture, influence the degree of laser energy-material coupling so that elements of the same abundance in a dissimilar matrices will produce different emission intensities because of changes in the amount of sample ablated into the plasma with each laser pulse [78,79]. Further discussion of physical matrix effects is beyond the scope of this paper but has been described in detail in numerous previous studies, e.g., [31,36,78,80–88]. Chemical matrix efects are more readily ameliorated through optimization of the LIBS analytical system than physical matrix effects [32] which, therefore, present the greatest challenge to, and impediment for, quantitative analysis of geomaterials by LIBS. Despite these complications, quantitative analysis is possible by LIBS, but to do so requires careful selection of emission lines and creation of univariate or multivariate calibration curves using physically and compositionally similar matrix-matched standards.

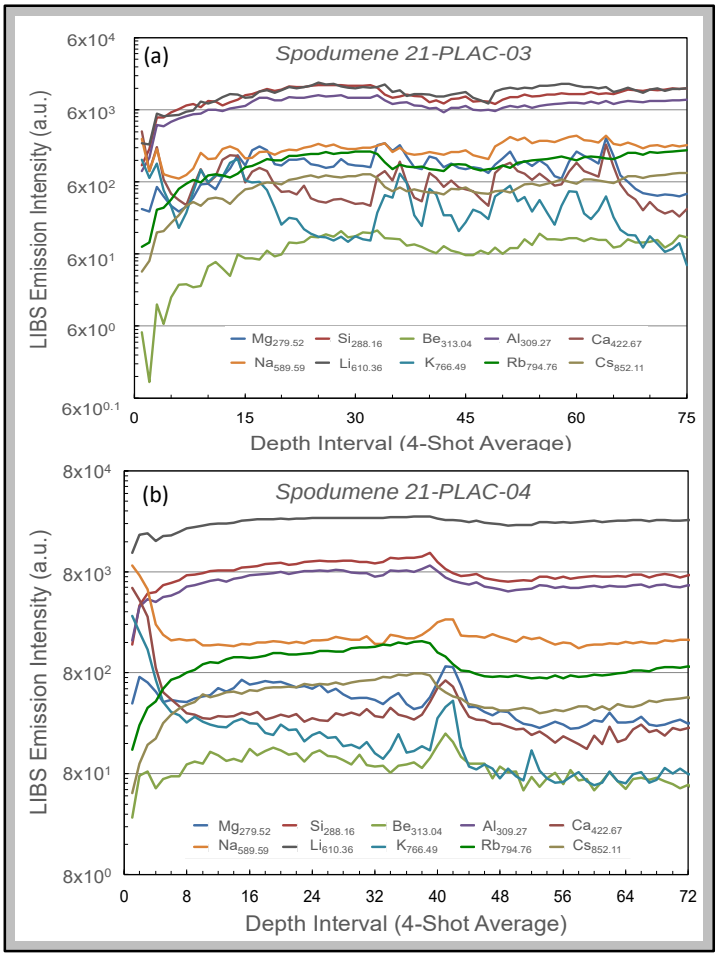

Figure 10. Depth profiles illustrating compositional variations just below the surface in two spodumene crystals from outcrops 21-PLAC-03 and 21-PLAC-04 on the Carolina Lithium Project prospect in Gaston County, N.C. Emission intensities are displayed for 10 elements (Mg, Si, Be, Al, Ca, Na, Li, K, Rb, and Cs) for 300 successive laser shots at a single spot on spodumene 21-PLAC-03 grouped into 4-shot averages (**a**) and 288 successive laser shots at a single spot on spodumene 21-PLAC-04 also grouped into 4-shot averages (**b**).

Quantitative analysis can be accomplished using *Geochem* mode of the Z-300 analyzer developed beforehand from the analysis of a set of matrix-matched reference materials using either single-element or multivariate calibration procedures. Two general calibrations curves are installed on Z-300 analyzers purchased for geoscience applications; a general geochemistry calibration ("geochem") based on >70 different geological materials and NIST standards and an iron ore calibration ("Fe ore") based on a smaller number of OREAS 400 series standard reference materials. Additionally, users can create bespoke calibration curves using the Z-300 *Profile Builder* PC-based software package as described in Harmon et al. [37].

Creating Z-300 calibrations utilizes a concentration versus intensity ratio approach that depends on two considerations: the number spectral lines for an element of interest and the presence of distinct emission lines that are not affected by overlap with lines from other elements present in the sample. Any LIBS calibration curve will perform best when developed for a specific matrix of interest. First, intensity values for elements are calculated after performing a Savitsky-Golay smoothing [89] on the LIBS spectrum, followed by a background subtraction, and finally integration of measured emission intensities across the defined spectral region of interest (ROI) to obtain a summed area under the peak value. Intensity ratios are then calculated by combining one or more summed peak intensity

values for the analyte element of interest in the numerator of the ratio and the denominator consisting either of the emission intensity for a single element or the sum of emission intensities of multiple elements for complex matrices. Ideally, elements used in the denominator comprise the bulk of the sample composition and remain relatively constant from sample to sample. Whilst concentration values are required for each of the target elements for which the calibration is being developed, they are not required for the elements in the denominator as elements of approximately constant composition (e.g., Al, Si and other major elements in silicate minerals) are used for this spectral intensity normalization. Once a set of calibration curves has been constructed, subsequent LIBS analysis using the Z-300 in the *Geochem* mode will calculate and display elemental concentrations for a test sample in real time.

As noted above, two provisional calibration curves have been developed on the Z-300 instrument from our initial work at the CLP prospect to illustrate this capability. These calibrations will be refined and enhanced, and new calibrations for other minerals developed, as our study continues and more samples of known composition are acquired. The first calibration (Figure 11) is for a set of mica samples with Li contents ranging from 0.014 to 2.59 wt. % from the collection of the U.S. Smithsonian Institution National Museum of Natural History that represent different LCT pegmatite subtypes and encompass a broad range of lithologies and geologic settings [90]. The second calibration (Figure 12) is for a suite of pressed pellets from 17 pulverized pegmatite core samples representing 1-m intervals in three drill holes on the CLP prospect previously analyzed by X-ray fluorescence (XRF) and inductively coupled plasma mass spectrometry (ICPMS). Low- and high-range calibration curves were developed for these samples, which ranged in Li content from 0.015 to 1.12 wt. %. Li contents measured for minerals, drill core, and soil from across the CLP prospect with the Z-300 handheld LIBS analyzer using these calibrations ranged from 0.005–2.672 wt. % (Table A3).

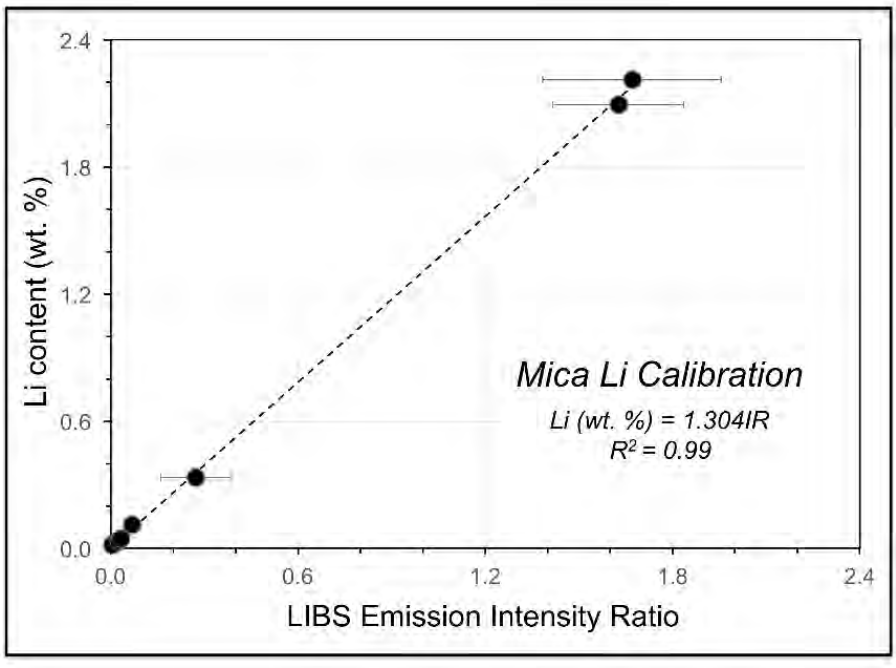

Figure 11. Handheld LIBS calibration curve for mica using the suite of nine mica specimens of known composition described in Table A1. The RMSE of the calibration is 0.0204%.

The calibration spectra were acquired with the same laser raster and pulse settings of 12 locations with two cleaning pulses and four data acquisition pulses per location. The laser was pulsed at a rate of 50 Hz and detector gating was used to avoid the collection of continuum light emitted early in the plasma lifetime, thus producing sharper spectra

with lower background. All 48 data pulses were averaged to produce a single spectrum for calibration use. Each sample was analyzed five times in this way and resulting intensity ratios were averaged. For the mica calibration, the Li intensity ratio consisted of the Li peak at 610.36 nm in the numerator and the sum of the peaks for Al at 394.40 nm, Ca at 396.85 nm, and Na at 819.48 nm in the denominator. The pegmatite powder calibration for our work at the CLP prospect used the intensity of Li nm peak at 610.36 nm in the numerator that was normalized to a combination of the intensities for the Al peak at 394.40 nm and the Fe peak at 438.35 nm.

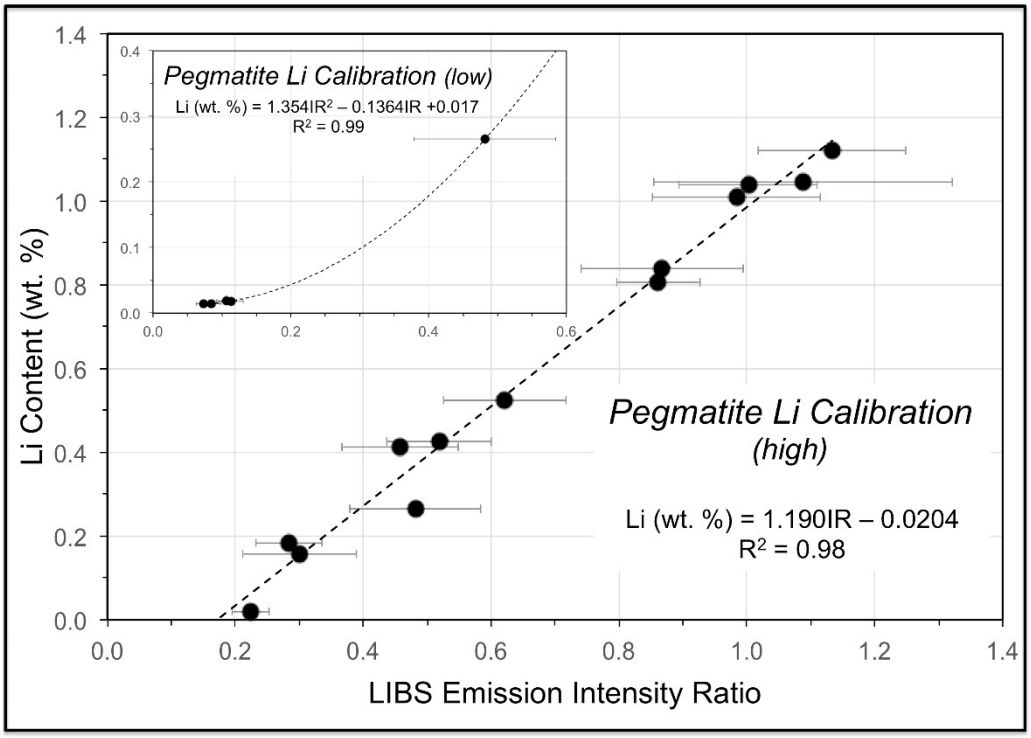

Figure 12. Handheld LIBS calibration curve developed from analysis of 18 pulverized pegmatite core samples from the CLP prospect described in Table A2. The RMSE values for the high and low calibrations are 0.0465% and 0.0021%, respectively.

Figure 13a shows the Z-300 *Geochem* mode screen display of LIBS spectra and sample Li composition of a muscovite from pegmatite outcrop sample 21-PLAC-02 and a surface exposure of the Cecil soil on the CLP prospect determined by comparison of an analyzed sample against the calibration that is provided to the analyst in real time.

The pegmatite powder calibration (Figure 12) was validated by analysis of a set of 14 pelletized powdered pegmatite samples from the Kleiber Oy Li deposit in Kaustinen-Kokkola area of central Ostrabothnia in western Finland, where Paleoproterozoic albite-spodumene pegmatites crosscut the Pohjanmaa schist belt situated between the Central Finland Granite and Vaasa Migmatite Complex of the Svecofennian Orogen [91,92]. Li contents for this validation suite range from 0.01–1.12 wt. % and, as shown in Table 2, analysis of the Kleiber Oy pegmatite powders against the calibration for the CLP pegmatite powders yielded Li contents very close to the assay values ($Li_{LIBS} = 0.941Li_{assay}$, $R^2 = 0.97$).

Figure 13. Screen shots from the Z-300 *Geochem* mode for a muscovite from Carolina Lithium Project prospect pegmatite outcrop sample 21-PLAC-02 (**a**) and a surface exposure of the Cecil soil on the CLP prospect (**b**). The Z-300 screenshots show the broadband LIBS spectrum recorded for each sample and estimated elemental abundances derived from the spectral emission line intensities. The Li content for the muscovite was determined from the mica calibration of Figure 11, whereas that for the Cecil soil was determined from the pegmatite powder calibration of Figure 12.

Table 2. Comparison of measured Li contents (wt. %) for pegmatite powders from the Kleiber Oy Li deposit, Finland with estimates using the CLP pegmatite powder calibration.

Sample #	**KOP-21**	**KOP-22**	**KOP-23**	**KOP-24**	**KOP-25**	**KOP-26**	**KOP-27**
Assay Li content	0.048	0.630	0.394	0.837	0.527	0.003	0.004
LIBS predicted Li content	0.046	0.703	0.322	0.856	0.484	0.002	0.003
Sample #	**KOP-28**	**KOP-29**	**KOP-30**	**KOP-31**	**KOP-32**	**KOP-36**	**KOP-40**
Assay Li content	0.214	0.746	0.251	0.863	1.016	0.608	0.009
LIBS predicted Li content	0.089	0.684	0.278	0.843	1.112	0.777	0.011

This example shows that calibrations for quantification can be developed using hand-held LIBS in situations of appropriate matrix matching between standards and samples. But what if that isn't possible? We considered this through analysis of a dozen samples from soil core 20-BD-359 from the CLP prospect drilled through the Cecil soil into saprolite. The Cecil soil is a well drained and moderately permeable soil derived from the deep weathering of felsic, igneous and high-grade metamorphic rocks on uplands throughout the Piedmont region of North Carolina [93] that is comprised primarily of Al and Fe oxy-hydroxide minerals [94] rather than the aluminosilicate matrix on which the pegmatite powder calibration is based. The soil core samples, which were prepared as pressed pellets in exactly the same way as the pulverized pegmatites, were analyzed using both our pegmatite powder calibration and the SciAps general geochemistry calibration. Neither calibration produced the robust results shown in Table 2 for the Kleiber Oy pegmatite powders, but the latter yielded a more statistically significant relationship between Li assay values and LIBS abundance estimates than the former: $Li_{LIBS} = 0.828Li_{assay}$, $R^2 = 0.18$ using the pegmatite powder calibration versus $Li_{LIBS} = 0.368Li_{assay}$, $R^2 = 0.52$ using the Z-300 general geochemistry calibration. As illustrated in Table 3, soil Li abundances are closer to actual values for this general geochemistry calibration, which is based on >70 different geological materials that include a variety of soils, than for the calibration derived solely from the pegmatite powder which has an aluminosilicate matrix. A similar situation is observed when the suite of micas used to develop the mica calibration is analysed using

the pegmatite powder calibration (Table 4), with Li abundances lower using the pegmatite powder calibration than with the mica calibration. These two examples highlight the importance of matrix matching for quantitative LIBS.

Table 3. Comparison of Li analysis for a soil core on the Carolina Lithium Project prospect using different calibrations (CAL). PP = pegmatite powder, SAGG = SciAps General Geochemistry.

Z-300 ID	Sample Number	Li Assay (wt. %)	LIBS Li (wt. %)	CAL	Z-300 ID	Sample Number	Li Assay (wt. %)	LIBS Li (wt. %)	CAL
392	E00097886	0.023	0.009	PP	473	E00097886	0.023	0.014	SAGG
395	E00097887	0.049	0.018	PP	475	E00097887	0.049	0.032	SAGG
398	E00097888	0.035	0.018	PP	477	E00097888	0.035	0.022	SAGG
401	E00097889	0.043	0.02	PP	479	E00097889	0.043	0.031	SAGG
404	E00097890	0.030	0.008	PP	481	E00097890	0.030	0.025	SAGG
407	E00097891	0.039	0.015	PP	483	E00097891	0.039	0.049	SAGG
410	E00097892	0.022	0.006	PP	486	E00097892	0.022	0.024	SAGG
413	E00097893	0.030	0.012	PP	488	E00097893	0.030	0.033	SAGG
416	E00097894	0.036	0.012	PP	490	E00097894	0.036	0.035	SAGG
419	E00097895	0.029	0.012	PP	492	E00097895	0.029	0.031	SAGG
422	E00097896	0.033	0.013	PP	494	E00097896	0.033	0.030	SAGG
425	E00098117	0.033	0.005	PP	496	E00098117	0.033	0.011	SAGG

Table 4. Li analysis of mica using the mica (MC) and pegmatite powder (PP) calibrations.

Z-300 IDs	Sample Number	Li_{MC} (wt. %)	Li_{PP} (wt. %)
292 & 293	21-PLAC-02	0.091	0.007
306 & 307	Mt. Mica-11	1.357	1.159
341 & 342	Mt. Mica-56	0.052	0.005
361 & 362	Mt. Marie-15	0.052	0.004
376 & 377	Brown Derby Mine	1.943	1.437
433 & 434	Grosmont	1.842	1.75
456 & 457	Viitaniemi	2.202	0.008

6.4. Lithium Geochemistry for Exploration

Elevated values of Li in muscovite can suggest the presence of Li-bearing assemblages in LCT pegmatite populations. Lithium can substitute in the octahedral site of the muscovite structure via coupled substitutions involving Si, Al and vacancies [95,96]. The absolute value of Li in muscovite from granitic pegmatites can be as high as 3 wt. % Li, however, a minimal threshold of approximately 0.05 wt. % serves as a guide to prospecting for spodumene-bearing pegmatites [97]. Evolved muscovite compositions in LCT pegmatites generally show low K/Rb ratios and high Li contents with fractionation trends characterized by decreasing K/Rb with increasing Li contents.

Muscovite samples from the CLP prospect analyzed by the Z-300 handheld LIBS analyzer show reasonably high Li contents of 0.107–0.186 wt. % (Table A1), but does not reach the >1.5 wt. % levels observed for lepidolite [98]. K/Rb ratios calculated from the $K_{766.43}$ and $Rb_{779.97}$ spectral emission lines range from 3.0–8.6. As seen in Figure 14, our data for the CLP prospect plots within the mineralized field of granitic pegmatites and compares quite favorably to the domain of muscovite compositions from spodumene- and petalite-bearing pegmatites determined from other studies. The K/Rb and Li data for muscovites from the CLP prospect confirm the highly fractionated nature of these spodumene-bearing pegmatites. This approach to identifying fractionated LCT pegmatites has wide potential for rapidly identifying mineralized pegmatites by the exploration geologist in the field, as both Li content and K/Rb ratio can be calculated in real time by on-board software from a single LIBS mica analysis.

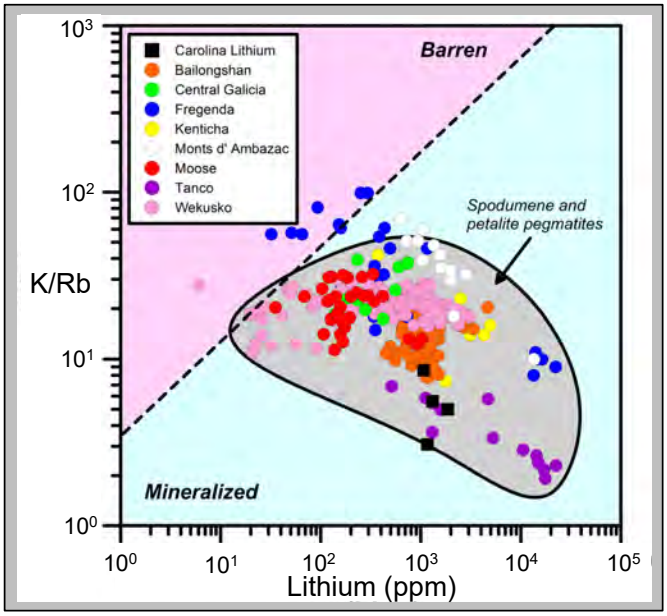

Figure 14. Comparison of muscovite K/Rb-Li (ppm) systematics for the CLP prospect with muscovite K/Rb-Li relationships for other Li-pegmatites worldwide: Bailongshan field, China [99]; Central Galicia field, Spain [100]; Fregenda area, Spain [101]; Kenticha pegmatite, Ethiopia [102]; Monts d' Ambazac field, France [103]; Moose pegmatite, Northwest Territories, Canada [104]; Tanco pegmatite, Manitoba, Canada [105]; and Dike 1, Wekusko Lake field, Manitoba, Canada [106].

7. Summary and Conclusions

LIBS is an analytical technique that has long been used for the analysis of ore minerals in laboratory [107–111] and, more recently, bespoke industrial LIBS systems have been developed for mineral exploration and exploitation [71,112–116]. The rapid acquisition of compositional data afforded by LIBS facilitates the interpretation of geochemical data in exploration, prospect evaluation, and ore processing contexts. Commercial handheld LIBS was developed in 2016 [34] and its potential for use in resources exploration was demonstrated shortly thereafter [37,46,48,117]. Here, we have described and illustrated the different analytical capabilities of handheld LIBS for mineral exploration, demonstrating elemental detection, microchemical mapping, depth profiling, and quantitative analysis with specific examples drawn from our analysis of soil, rocks, outcrops, and drill core from an active Li prospect in North Carolina (USA).

Using qualitative elemental analysis, the LIBS can differentiate minerals with similar field appearance such as muscovite and lepidolite and can identify accessory minerals like tourmaline and secondary minerals such as vivianite. Through microchemical mapping we illustrated how LIBS provides information about chemical homogeneity or heterogeneity at the 10s of micron spatial scale, yielding useful insights into coupled or decoupled behavior of elements within a sample. Similarly, the depth profiling ability of LIBS can be used to observe elemental distributions below the surface, allowing recognition of the effects of surficial weathering, a change in mineralogy, and presence of inclusions. Using laboratory-derived calibrations prior to fieldwork, quantitative chemical abundances in rocks, minerals, and soils can be readily measured in the field by handheld LIBS. Our new data both demonstrate the reliability of such calibrations and document the importance of having matrix matching when using a calibration. Finally, we illustrated the ability of handheld LIBS to effectively measure K/Rb and Li contents of muscovite, which has the potential for on-site recognition of the barren or fertile nature of the host pegmatite with regards to Li-enrichment. This is vital in an exploration or evaluation situation where spodumene might not be present on the surface outcrop of a pegmatite, but other minerals like muscovite are still available for chemical analysis. Overall, our study demonstrates

the ability of LIBS to provide rapid geochemical analyses in support of Li exploration of LCT pegmatites, which has the potential to save exploration endeavors money, time, and resources.

Author Contributions: M.A.W. and R.S.H. defined the study. R.S.H. and M.J. undertook the laboratory analyses prior to the fieldwork and developed the Li calibrations for the Z-300. A.C., R.S.H., and Z.G. conducted the LIBS analysis, with D.K. assisting with post-analysis spectral preprocessing. M.A.W., R.S.H., A.C. and M.J. prepared the paper with review from all co-authors. All authors have read and agreed to the published version of the manuscript.

Funding: Funding for the purchase of the Z-300 LIBS analyzer was provided to Professor Lewis A. Owen, Chair of the Department of Marine, Earth, and Atmospheric Sciences, by North Carolina State University.

Data Availability Statement: The LIBS spectra for all of the samples described in this paper are archived in the Li Pegmatite Project folder on the Open Science Framework at https://www.osf.io/zhr9x/ (accessed on 2 January 2022).

Acknowledgments: Our appreciation is extended to Piedmont Lithium, Inc., specifically Lamont Leatherman, Michael Mason, and Gretchen Williams for logistical support, provision of geochemical data and for facilitating the in-field portion for this study, and to Lamont Leatherman and Patrick Brindle for internal review of the paper. This paper was improved by the thorough and insightful review received from Cécile Fabre (U Lorraine).

Conflicts of Interest: The authors declare no conflict of interest.

Appendix A

Table A1. Minerals analyzed by handheld LIBS on the Piedmont Lithium Carolina Lithium Project prospect, Gaston County, N.C. (USA).

Sample Number	Description
Mica	
PL_21-BD-490	Coarse muscovite rosette in barren pegmatite drill core
PL_S2L1_21-PLAC-01	Muscovite in East Pit Steep pegmatite outcrop
PL_S2L2_21-PLAC-03	Muscovite in pegmatite outcrop
Quartz	
PL_18-BD-228	Quartz crystal in pegmatite drill core
PL_21-BD-490	Quartz crystal in pegmatite drill core
PL_S2L2_21-PLAC-03	Quartz crystal in pegmatite outcrop
PL_S4L1	Quartz crystal in pegmatite outcrop
PL_S4L2_21-PLAC-06	Quartz crystal in pegmatite outcrop
Feldspar	
PL_21-BD-446	Albite crystal in pegmatite drill core
PL_17-BD-46	100 cm-long feldspar crystal in pegmatite drill core
PL_17-BD-62	Feldspar crystal in pegmatite drill core
PL_18-BD-228	Feldspar crystal in pegmatite drill core
PL_S2L1_21-PLAC-03	K-feldspar crystal in pegmatite outcrop
PL_S3L1	Feldspar crystal in pegmatite outcrop
PL_S3L2	K-feldspar crystal in pegmatite outcrop
PL_S3L2	Plagioclase crystal in pegmatite outcrop
PL_S3L2	Albite crystal in pegmatite outcrop
PL_S4L1	K-feldspar crystal in surface float
PL_S4L1	Albite crystal in surface float
Spodumene	
PL 21-BD-444	Spodumene in pegmatite drill core
PL 17-BD-46	70-cm spodumene in pegmatite drill core
PL hand specimen-1	Altered spodumene in saprolitic pegmatite
PL_D0017573	Spodumene in sample D0017573
PL_S2L1_21-PLAC-01	Spodumene in East Pit Steep pegmatite
PL_S2L2_21-PLAC-03-1	Spodumene in pegmatite outcrop
PL_S2L2_21-PLAC-03-2	Spodumene in pegmatite outcrop
PL-S2L3_21-PLAC-04	Spodumene in pegmatite outcrop
PL_S2L1	Spodumene in surface float
PL_S4L2_21-PLAC-06-1	Spodumene in pegmatite outcrop
PL_S4L2_21-PLAC-06-2	Spodumene in pegmatite outcrop
Other Minerals	
PL_18-BD-228	Vivianite on fracture surface in drill core
PL_21BD-490	Fluorapatite in in drill core
PL_S3L2	Tourmaline in pegmatite outcrop

Table A2. Chemical analyses for mica calibration and pegmatite powder calibration curves (values in wt. %).

LCT Pegmatite Micas		Element							
Sample ID	**Locality**	**Li**	**K**	**Rb**	**Cs**				
Willis-7	Willis Warren, ME, USA	0.014							
Willis-2	Willis Warren, ME USA	0.033							
Mt Marie-15	Mt. Marie, Paris, ME, USA	0.042							
Mt Mica-56	Mt Mica, Paris, ME, USA	0.107							
Mt Mica-11	Mt Mica, Paris, ME, USA	0.334							
NMNH-165134	Bikita, Zimbabwe	1.779							
NMNH-105719	Brown Derby, CO, USA	2.088	8.388	1.712	0.071				
NMNH-R11827	Vitaniemi, Eräjärvi, Finland	2.209	8.733	0.778	0.271				
NMNH-128243	Grosmont, Western Australia, Australia	2.589	8.752	1.054	0.118				
Drill Core Pegmatite Powders, Carolina Lithium Project Prospect									
Sample ID	**Locality**	**Li**	**SiO_2**	**Al_2O_3**	**Fe_2O_3**	**MgO**	**CaO**	**Na_2O**	**K_2O**
20-BD-359 E00098037	Gaston County, NC (USA)	1.120	75.020	16.28	1.68	0.06	0.20	1.77	1.98
21-BD-413 F00097299	Gaston County, NC (USA)	1.046	75.920	16.18	1.21	0.01	0.20	2.88	1.90
21-BD-413 F00097290	Gaston County, NC (USA)	1.040	72.140	18.37	0.83	0.02	0.23	2.46	3.98
21-BD-398 F00098075	Gaston County, NC (USA)	1.010	74.490	15.89	1.40	0.09	0.25	1.91	2.40
21-BD-413 F00097297	Gaston County, NC (USA)	0.943	75.300	16.11	1.07	0.05	0.21	3.45	1.58
21-BD-413 F00097301	Gaston County, NC (USA)	0.839	73.640	16.69	0.95	0.04	0.30	3.98	1.89
20-BD-359 E00098047	Gaston County, NC (USA)	0.806	74.430	15.87	1.19	0.03	0.39	3.26	2.45
21-BD-398 F00098077	Gaston County, NC (USA)	0.526	74.170	15.16	1.25	0.09	0.44	3.64	2.62
20-BD-359 E00098045	Gaston County, NC (USA)	0.425	74.060	16.27	1.55	0.06	39.00	3.08	2.49
21-BD-398 F00098074	Gaston County, NC (USA)	0.441	74.510	15.55	0.96	0.05	0.29	5.19	2.06
20-BD-359 E00098043	Gaston County, NC (USA)	0.265	72.670	16.23	1.10	0.15	0.49	4.42	3.34
21-BD-398 F00098078	Gaston County, NC (USA)	0.185	75.020	15.08	0.93	0.06	0.31	5.40	1.75
20-BD-359 E00098033	Gaston County, NC (USA)	0.158	66.330	19.08	2.53	0.97	0.00	0.38	4.41
21-BD-413 F00097310	Gaston County, NC (USA)	0.021	72.700	15.44	0.92	0.16	1.53	6.90	0.98
21-BD-413 F00097275	Gaston County, NC (USA)	0.018	73.720	15.99	0.78	0.06	0.27	4.00	2.69
21-BD-413 F00097277	Gaston County, NC (USA)	0.018	73.000	15.78	0.66	0.07	0.52	5.70	2.95
21-BD-398 F00098065	Gaston County, NC (USA)	0.015	76.670	14.71	1.33	0.12	1.13	3.91	1.88
20-BD-359 E00098451	Gaston County, NC (USA)	0.014	72.830	15.92	1.03	0.19	0.60	3.54	6.38

Table A3. Li contents (wt. %) determined for minerals, drill core, and soil from the CLP prospect by handheld LIBS using the Z-300 handheld LIBS (M = mica calibration, PP = pegmatite powder calibration, GG = SciAps general geochemistry calibration).

Z-300 ID	Sample Description	Comment	Li (wt. %)	Cal
test 194	PL core—21-BD-490	mica in coarse mica rosette in barren pegmatite	0.118	M
test 196	PL core—21-BD-490	mica in coarse mica rosette in barren pegmatite	0.096	M
test 197	PL core—21-BD-490	mica in coarse mica rosette in barren pegmatite	0.137	M
test 200	PL core—21-BD-490	mica in mineralized pegmatite	0.204	M
test 202	PL core—21-BD-490	mica in mineralized pegmatite	0.189	M
test 203	PL core—21-BD-490	mica in mineralized pegmatite	0.205	M
test 204	PL core—hole 21-BD-444	spodumene in barren pegmatite	0.142	PP
test 205	PL core—hole 21-BD-444	spodumene in barren pegmatite	0.143	PP
test 206	PL core—hole 21-BD-444	spodumene in barren pegmatite	0.140	PP
test 207	PL core—hole 21-BD-444	mineralized pegmatite	0.298	PP
test 208	PL core—hole 21-BD-444	mineralized pegmatite	0.435	PP
test 213	PL core—hole 21-BD-444	mineralized pegmatite	0.282	PP
test 218	PL core 18-BD-228	quartz	0.053	PP
test 221	PL core 18-BD-228	quartz	0.418	PP
test 224	PL core 18-BD-228	quartz	0.117	PP
test 226	PL core 18-BD-228	feldspar	0.011	PP
test 227	large hand specimen	altered spodumene in saprolite	0.006	PP
test 230	PL core—21-BD-490	quartz	0.162	PP

Table A3. *Cont.*

Z-300 ID	Sample Description	Comment	Li (wt. %)	Cal
test 243	21-PLAC-01	mica; East Pit Steep	0.186	M
test 245	21-PLAC-01	spodumene; East Pit Steep	2.672	PP
test 246	21-PLAC-02	spodumene; East Pit Steep	1.603	PP
test 247	21-PLAC-02	spodumene; East Pit Steep	1.972	PP
test 248	21-PLAC-02	spodumene; East Pit Steep	0.984	PP
test 249	21-PLAC-02	spodumene; East Pit Steep	0.979	PP
test 250	21-PLAC-02	spodumene; East Pit Steep	1.153	PP
test 251	21-PLAC-03	Spodumene-1	2.671	PP
test 252	21-PLAC-03	Spodumene-2	1.377	PP
test 253	21-PLAC-03	Spodumene-2	1.505	PP
test 254	21-PLAC-03	large mica	0.126	M
test 255	21-PLAC-03	large mica	0.137	M
test 256	21-PLAC-04	spodumene	1.015	PP
test 257	21-PLAC-04	spodumene	1.573	PP
test 258	Stop 2	soil on road	0.006	PP
test 261	Stop 2	Na-feldspar float in soil	0.010	PP
test 263	Stop 2	quartz float in soil	0.021	PP
test 264	21-PLAC-06	spodumene	1.800	PP
test 472	PL core 20-SBD-017	soil core 1.2–2.4 m	0.009	PP
test 473	PL core 20-SBD-017	soil core 1.2–2.4 m	0.014	GG
test 474	PL core 20-SBD-017	soil core 2.4–4.0 m	0.017	PP
test 475	PL core 20-SBD-017	soil core 2.4–4.0 m	0.032	GG
test 476	PL core 20-SBD-017	soil core 4.0–5.5 m	0.018	PP
test 477	PL core 20-SBD-017	soil core 4.0–5.5 m	0.022	GC
test 478	PL core 20-SBD-017	soil core 5.5–8.5 m	0.020	PP
test 479	PL core 20-SBD-017	soil core 5.5–8.5 m	0.031	GG
test 480	PL core 20-SBD-017	soil core 8.5–10.0 m	0.008	PP
test 481	PL core 20-SBD-017	soil core 8.5–10.0 m	0.025	GG
test 482	PL core 20-SBD-017	soil core 10.0–11.5 m	0.059	PP
test 483	PL core 20-SBD-017	soil core 10.0–11.5 m	0.049	GG
test 485	PL core 20-SBD-017	soil core 11.5–13.1 m	0.006	PP
test 486	PL core 20-SBD-017	soil core 11.5–13.1 m	0.024	GG
test 487	PL core 20-SBD-017	soil core 13.1–14.6 m	0.018	PP
test 488	PL core 20-SBD-017	soil core 13.1–14.6 m	0.033	GG
test 489	PL core 20-SBD-017	soil core 14.6–16.2 m	0.012	PP
test 490	PL core 20-SBD-017	soil core 14.6–16.2 m	0.035	GG
test 491	PL core 20-SBD-017	soil core 16.2–17.6 m	0.012	PP
test 492	PL core 20-SBD-017	soil core 16.2–17.7 m	0.031	GG
test 493	PL core 20-SBD-017	soil core 17.7–19.2 m	0.013	PP
test 494	PL core 20-SBD-017	soil core 17.7–19.2 m	0.030	GG
test 495	PL core 20-SBD-017	soil core 19.2–20.7 m	0.005	PP
test 496	PL core 20-SBD-017	soil core 20.7–22.3 m	0.011	GG

References

1. USGS. *Mineral Commodity Summary 2011: Lithium*; U.S. Geological Survey: Reston, VA, USA, 2011. [CrossRef]
2. Teng, F.-Z.; McDonough, W.; Rudnick, R.; Dalpé, C.; Tomascak, P.; Chappell, B.; Gao, S. Lithium isotopic composition and concentration of the upper continental crust. *Geochim. Cosmochim. Acta* **2004**, *68*, 4167–4178. [CrossRef]
3. Gruber, P.W.; Medina, P.A.; Keoleian, G.A.; Kesler, S.E.; Everson, M.P.; Wallington, T.J. Global Lithium Availability: A constraint for electric vehicles? *J. Ind. Ecol.* **2011**, *15*, 760–775. [CrossRef]
4. Grosjean, C.; Miranda, P.H.; Perrin, M.; Poggi, P. Assessment of world lithium resources and consequences of their geographic distribution on the expected development of the electric vehicle industry. *Renew. Sustain. Energy Rev.* **2012**, *16*, 1735–1744. [CrossRef]
5. Kesler, S.E.; Gruber, P.W.; Medina, P.A.; Keoleian, G.A.; Everson, M.P.; Wallington, T.J. Global lithium resources: Relative importance of pegmatite, brine and other deposits. *Ore Geol. Rev.* **2012**, *48*, 55–69. [CrossRef]
6. Kavanagh, L.; Keohane, J.; Garcia Cabellos, G.; Lloyd, A.; Cleary, J. Global Lithium Sources—Industrial Use and Future in the Electric Vehicle Industry: A Review. *Resources* **2018**, *7*, 57. [CrossRef]

7. Linnen, R.L.; Van Lichtervelde, M.; Černý, P. Granitic Pegmatites as Sources of Strategic Metals. *Elements* **2012**, *8*, 275–280. [CrossRef]
8. Černý, P.; Ercit, S. The classification of granitic pegmatites revisited. *Can. Mineral.* **2005**, *43*, 2005–2026. [CrossRef]
9. Černý, P.; London, D.; Novak, M. Granitic pegmatites as reflections of their sources. *Elements* **2012**, *8*, 289–294. [CrossRef]
10. Simmons, W.; Falster, A.; Webber, K.; Roda-Robles, E.; Boudreaux, A.P.; Grassi, L.R.; Freeman, G. Bulk composition of Mt. Mica pegmatite, Maine, USA: Implications for the origin of an LCT type pegmatite by anatexis. *Can. Miner.* **2016**, *54*, 1053–1070. [CrossRef]
11. Barros, R.; Menuge, J.F. The origin of spodumene pegmatites associated with the Leinster Granite in southeast Ireland. *Can. Miner.* **2016**, *54*, 847–862. [CrossRef]
12. Fuchsloch, W.C.; Nex, P.A.; Kinnaird, J.A. Classification, mineralogical and geochemical variations in pegmatites of the Cape Cross-Uis pegmatite belt, Namibia. *Lithos* **2018**, *296–299*, 79–95. [CrossRef]
13. Černý, P.; Meintzer, R.E. Fertile granites in the Archean and Proterozoic fields of rare-element pegmatites: Crustal environment, geochemistry, and petrogenetic relationships. In *Recent Advances in the Geology of Granite Related Mineral De-Posits*; Canadian Institute of Mining and Metallurgy: Montreal, QC, Canada, 1988; Volume 39, pp. 170–207.
14. Baker, D.R. The escape of pegmatite dikes from granitic plutons; constraints from new models of viscosity and dike propagation. *Can. Mineral.* **1998**, *36*, 255–263.
15. Černý, P. Characteristics of pegmatite deposits of tantalum. In *Lanthanides, Tantalum and Niobium*; Černý, P., Möller, P., Saupe, F., Eds.; Springer: Berlin/Heidelberg, Germany, 1989; pp. 195–239.
16. Černý, P.; Meintzer, R.E.; Anderson, A.J. Extreme fractionation in rare-element granitic pegmatites; selected ex-amples of data and mechanisms. *Can. Mineral.* **1985**, *23*, 381–421.
17. Trueman, D.L.; Černý, P. Granitic pegmatites in science and industry. In *Short Course Handbook*; Mineralogical Association of Canada: Quebec City, QC, Canada, 1982; Volume 8, p. 463.
18. Kish, S.A.; Fullagar, P.D. Age and magmatic association of rare metal pegmatites; spodumene pegmatites, Kings Mountain, NC and Sn–Ta pegmatites, Rockford, Ala. *Geol. Soc. Am. Abstr. Programs* **1996**, *28*, A475.
19. Horton, J.W.; Butler, J.R. The Kings Mountain belt and spodumene pegmatite district, Cherokee and York Counties, South Carolina, and Cleveland County, North Carolina. In *Centennial Field Guide*; Neathery, T.L., Ed.; Southeastern Section of the Geological Society of America: Boulder, CO, USA, 1986; Volume 6, pp. 239–244.
20. Horton, J.W. Shear zone between the Inner Piedmont and Kings Mountain belts in the Carolinas. *Geology* **1981**, *9*, 28. [CrossRef]
21. Kesler, T. *The Tin-Spodumene Belt of the Carolinas, a Preliminary Report*; U.S. Government Printing Office: Washington, DC, USA, 1942; 269p. [CrossRef]
22. Kesler, T.L. The Kings Mountain area. In *Guides to Southeastern Geology*; Russell, R.J., Ed.; Geological Society of America Field Trip Guidebook: Boulder, CO, USA, 1955; pp. 374–387.
23. Kesler, T.L. Occurrence, development, and long-range outlook of lithium-pegmatite ore in the Carolinas. In *Lithium Resources and Requirements by the Year 2000*; Vine, J.D., Ed.; U.S. Geological Survey Professional Paper 1005; 1976; pp. 45–50.
24. Luster, G.R. Lithologic Variability of the Kings Mountain Pegmatite, North Carolina. Master's Thesis, Pennsylvania State University, University Park, PA, USA, 1977.
25. Hodges, R.A. A Petrologic Study of the Lithium Corporation of America Mine in the Tin–Spodumene Belt of North Carolina. Master's Thesis, University of North Carolina, Chapel Hill, NC, USA, 1983.
26. Griffitts, W.R.; Overstreet, W.C. Granitic rocks of the western Carolina Piedmont. *Am. J. Sci.* **1952**, *250*, 777–789. [CrossRef]
27. Kesler, T.L. Exploration of the Kings Mountain pegmatites. *Miner. Eng.* **1961**, *13*, 1062–1068.
28. White, J.S. Mineralogy of the Foote mine, Kings Mountain, North Carolina. In *Geological Investigations of the Kings Mountain Belt and Adjacent Areas in the Carolinas*; Horton, J.W., Butler, J.R., Milton, D.M., Eds.; Carolina Geological Society Field Trip Guidebook; South Carolina Geological Survey: Columbia, SC, USA, 1981; pp. 39–48.
29. Swanson, S.E. Mineralogy of spodumene pegmatites and related rocks in the tin-spodumene belt of North Carolina and South Carolina, USA. *Can. Miner.* **2012**, *50*, 1589–1608. [CrossRef]
30. Kesler, T.L. Raw lithium supplies. *Min. Eng.* **1978**, *30*, 283–285.
31. Harmon, R.S.; Senesi, G.S. Laser-Induced Breakdown Spectroscopy—A geochemical tool for the 21st century. *Appl. Geochem.* **2021**, *128*, 104929. [CrossRef]
32. Cremers, D.A.; Radziemski, L.J. *Handbook of Laser-Induced Breakdown Spectroscopy*, 2nd ed.; John Wiley & Sons: Chichester, UK, 2013.
33. Pedarnig, J.D.; Trautner, S.; Grünberger, S.; Giannakaris, N.; Eschlböck-Fuchs, S.; Hofstadler, J. Review of element analysis of industrial materials by in-line laser-induced breakdown spectroscopy (LIBS). *Appl. Sci.* **2021**, *11*, 9274. [CrossRef]
34. Connors, B.; Somers, A.; Day, D. Application of handheld laser-induced breakdown spectroscopy (LIBS) to geochemical analysis. *Appl. Spectrosc.* **2016**, *70*, 810–815. [CrossRef] [PubMed]
35. Harmon, R.S.; Hark, R.R.; Throckmorton, C.S.; Rankey, E.C.; Wise, M.A.; Somers, A.M.; Collins, L.M. Geochemical fingerprinting by handheld laser-induced breakdown spectroscopy. *Geostand. Geoanal. Res.* **2017**, *41*, 563–584. [CrossRef]
36. Harmon, R.S.; Throckmorton, C.S.; Hark, R.R.; Gottfried, J.; Wörner, G.; Harpp, K.; Collins, L. Discriminating volcanic centers with handheld laser-induced breakdown spectroscopy (LIBS). *J. Archaeol. Sci.* **2018**, *98*, 112–127. [CrossRef]

37. Harmon, R.S.; Lawley, C.J.; Watts, J.; Harraden, C.L.; Somers, A.M.; Hark, R.R. Laser-induced breakdown spectroscopy—An emerging analytical tool for mineral exploration. *Minerals* **2019**, *9*, 718. [CrossRef]
38. Harmon, R.S.; Khashchevskaya, D.; Morency, M.; Owen, L.A.; Jennings, M.; Knott, J.R.; Dortch, J.M. Analysis of rock varnish from the Mojave Desert by handheld laser-induced breakdown spectroscopy. *Molecules* **2021**, *26*, 5200. [CrossRef] [PubMed]
39. Senesi, G. Portable handheld laser-induced breakdown spectroscopy (LIBS) instrumentation for in-field elemental analysis of geological samples. *Int. J. Earth Environ. Sci.* **2017**, *2*, 17. [CrossRef]
40. Senesi, G.S.; Harmon, R.S.; Hark, R.R. *Field Portable and Handheld LIBS: In Laser Induced Breakdown Spectroscopy*; Singh, J.P., Thakur, S.Y., Eds.; Elsevier: Amsterdam, The Netherlands, 2020; pp. 537–560.
41. Senesi, G.S.; Manzari, P.; Consiglio, A.; De Pascale, O. Identification and classification of meteorites using a handheld LIBS instrument coupled with a fuzzy logic-based method. *J. Anal. At. Spectrom.* **2018**, *33*, 1664–1675. [CrossRef]
42. Senesi, G.; Manzini, D.; De Pascale, O. Application of a laser-induced breakdown spectroscopy handheld instrument to the diagnostic analysis of stone monuments. *Appl. Geochem.* **2018**, *96*, 87–91. [CrossRef]
43. Senesi, G.S.; Manzari, P.; Tempesta, G.; Agrosì, G.; Touchnt, A.A.; Ibhi, A.; De Pascale, O. Handheld laser induced breakdown spectroscopy instrumentation applied to the rapid discrimination between iron meteorites and meteor-wrongs. *Geostand. Geoanal. Res.* **2018**, *42*, 607–614. [CrossRef]
44. Pochon, A.; Desaulty, A.-M.; Bailly, L. Handheld laser-induced breakdown spectroscopy (LIBS) as a fast and easy method to trace gold. *J. Anal. At. Spectrom.* **2020**, *35*, 254–264. [CrossRef]
45. Defnet, P.; Wise, M.; Harmon, R.; Hark, R.; Hilferding, K. Analysis of garnet by laser-induced breakdown spectroscopy—Two practical applications. *Minerals* **2021**, *11*, 705. [CrossRef]
46. Lawley, C.J.; Somers, A.M.; Kjarsgaard, B.A. Rapid geochemical imaging of rocks and minerals with handheld laser induced breakdown spectroscopy (LIBS). *J. Geochem. Explor.* **2020**, *222*, 106694. [CrossRef]
47. Lemière, B.; Harmon, R.S. *XRF and LIBS for Field Geology: In Portable Spectroscopy and Spectrometry: Technologies and Instrumentation*; Crocombe, R., Leary, P., Kammrath, B., Eds.; John Wiley & Sons: Hoboken, NJ, USA, 2021; pp. 457–499.
48. Fabre, C.; Ourti, N.; Mercadier, J.; Cardoso-Fernandes, J.; Dias, F.; Perrotta, M.; Koerting, F.; Lima, A.; Kaestner, F.; Koellner, N.; et al. Analyses of Li-rich minerals using handheld LIBS tool. *Data* **2021**, *6*, 68. [CrossRef]
49. Rammelkamp, K.; Schröder, S.; Ortenzi, G.; Pisello, A.; Stephan, K.; Baqué, M.; Hübers, H.-W.; Forni, O.; Sohl, F.; Thomsen, L.; et al. Field investigation of volcanic deposits on Vulcano, Italy using a handheld laser-induced breakdown spectroscopy instrument. *Spectrochim. Acta Part B At. Spectrosc.* **2021**, *177*, 106067. [CrossRef]
50. Harmon, R.S.; Remus, J.; McMillan, N.J.; McManus, C.; Collins, L.; Gottfried, J.; DeLucia, F.C.; Miziolek, A.W. LIBS analysis of geomaterials: Geochemical fingerprinting for the rapid analysis and discrimination of minerals. *Appl. Geochem.* **2009**, *24*, 1125–1141. [CrossRef]
51. Tucker, J.; Dyar, M.; Schaefer, M.; Clegg, S.; Wiens, R. Optimization of laser-induced breakdown spectroscopy for rapid geochemical analysis. *Chem. Geol.* **2010**, *277*, 137–148. [CrossRef]
52. Zorov, N.B.; Gorbatenko, A.A.; Labutin, T.A.; Popov, A. A review of normalization techniques in analytical atomic spectrometry with laser sampling: From single to multivariate correction. *Spectrochim. Acta Part B At. Spectrosc.* **2010**, *65*, 642–657. [CrossRef]
53. Dyar, M.D.; Giguere, S.; Carey, C.; Boucher, T. Comparison of baseline removal methods for laser-induced breakdown spectroscopy of geological samples. *Spectrochim. Acta Part B At. Spectrosc.* **2016**, *126*, 53–64. [CrossRef]
54. Yi, C.; Lv, Y.; Xiao, H.; Ke, K.; Yu, X. A novel baseline correction method using convex optimization framework in laser-induced breakdown spectroscopy quantitative analysis. *Spectrochim. Acta Part B At. Spectrosc.* **2017**, *138*, 72–80. [CrossRef]
55. Guezenoc, J.; Gallet-Budynek, A.; Bousquet, B. Critical review and advices on spectral-based normalization methods for LIBS quantitative analysis. *Spectrochim. Acta Part B At. Spectrosc.* **2019**, *160*, 105688. [CrossRef]
56. Fabre, C.; Boiron, M.-C.; Dubessy, J.; Chabiron, A.; Charoy, B.; Martin-Crespo, T. Advances in lithium analysis in solids by means of laser-induced breakdown spectroscopy: An exploratory study. *Geochim. Cosmochim. Acta* **2002**, *66*, 1401–1407. [CrossRef]
57. McMillan, N.J.; McManus, C.E.; Harmon, R.S.; De Lucia, F.C.; Miziolek, A.W. Laser-induced breakdown spectroscopy analysis of complex silicate minerals—Beryl. *Anal. Bioanal. Chem.* **2006**, *385*, 263–271. [CrossRef] [PubMed]
58. McManus, C.E.; McMillan, N.J.; Harmon, R.S.; Whitmore, R.C.; De Lucia, J.F.C.; Miziolek, A.W. Use of laser induced breakdown spectroscopy in the determination of gem provenance: Beryls. *Appl. Opt.* **2008**, *47*, G72–G79. [CrossRef]
59. Sweetapple, M.T.; Tassios, S. Laser-induced breakdown spectroscopy (LIBS) as a tool for in situ mapping and textural interpretation of lithium in pegmatite minerals. *Am. Mineral.* **2015**, *100*, 2141–2151. [CrossRef]
60. Romppanen, S.; Pölönen, I.; Häkkänen, H.; Kaski, S. Optimization of spodumene identification by statistical approach for laser-induced breakdown spectroscopy data of lithium pegmatite ores. *Appl. Spectrosc. Rev.* **2021**, 1–21. [CrossRef]
61. Janovszky, P.; Jancsek, K.; Palásti, D.J.; Kopniczky, J.; Hopp, B.; Tóth, T.M.; Galbács, G. Classification of minerals and the assessment of lithium and beryllium content in granitoid rocks by laser-induced breakdown spectroscopy. *J. Anal. At. Spectrom.* **2021**, *36*, 813–823. [CrossRef]
62. Ribeiro, R.; Capela, D.; Ferreira, M.; Martins, R.; Jorge, P.; Guimarães, D.; Lima, A. X-ray fluorescence and laser-induced breakdown spectroscopy analysis of Li-rich minerals in veins from Argemela Tin Mine, central Portugal. *Minerals* **2021**, *11*, 1169. [CrossRef]
63. Fabre, C. Advances in laser-induced breakdown spectroscopy analysis for geology: A critical review. *Spectrochim. Acta Part B At. Spectrosc.* **2020**, *166*, 105799. [CrossRef]

64. Shearer, K.C.; Papike, J.J.; Simon, B.S.; Laul, C.J. Pegmatite-wallrock interactions, Black Hills, South Dakota; interaction between pegmatite-derived fluids and quartz-mica schist wallrock. *Am. Mineral.* **1986**, *71*, 518–539.
65. Morgan, G.B.; London, D. Alteration of amphibolitic wallrocks around the Tanco rare-element pegmatite, Bernic Lake, Manitoba. *Am. Mineral.* **1987**, *72*, 1097–1121.
66. Galeschuk, C.; Vanstone, P. Exploration techniques for rare-element pegmatite in the Bird River greenstone belt, southeastern Manitoba. In Proceedings of the Exploration, 5th Decenial Conference on Mineral Exploration, Toronto, ON, Canada, 9–12 September 2007; Milkereit, B., Ed.; Volume 7, pp. 823–839.
67. Luecke, W. Soil geochemistry above a lithium pegmatite dyke at Aclare, Southeast Ireland. *Ir. J. Earth Sci.* **1984**, *6*, 205–211.
68. Marshall, B.T.; Herman, J.S. Trace element distribution in the soils above deeply weathered pegmatites, Virginia, U.S.A.: Implications for exploration. *Appl. Geochem.* **1986**, *1*, 681–690. [CrossRef]
69. Kramida, A.; Ralchenko, Y.; Reader, J.; NIST ASD Team. *NIST Atomic Spectra Database (Version 5.5.6)*; National Institute of Standards and Technology: Gaithersburg, MD, USA, 2021. Available online: https://physics.nist.gov/asd (accessed on 19 November 2021).
70. Noll, R.; Bette, H.; Brysch, A.; Kraushaar, M.; Mönch, I.; Peter, L.; Sturm, V. Laser-induced breakdown spectrometry—applications for production control and quality assurance in the steel industry. *Spectrochim. Acta Part B At. Spectrosc.* **2001**, *56*, 637–649. [CrossRef]
71. Noll, R.; Fricke-Begemann, C.; Brunk, M.; Connemann, S.; Meinhardt, C.; Scharun, M.; Sturm, V.; Makowe, J.; Gehlen, C. Laser-induced breakdown spectroscopy expands into industrial applications. *Spectrochim. Acta Part B At. Spectrosc* **2014**, *93*, 41–51. [CrossRef]
72. Noll, R.; Fricke-Begemann, C.; Connemann, S.; Meinhardt, C.; Sturm, V. LIBS analyses for industrial applications–an overview of developments from 2014 to 2018. *J. Anal. At. Spectrom.* **2018**, *33*, 945–956. [CrossRef]
73. Sturm, V.; Vrenegor, J.; Noll, R.; Hemmerlin, M. Bulk analysis of steel samples with surface scale layers by enhanced laser ablation and LIBS analysis of C, P, S, Al, Cr, Cu, Mn and Mo. *J. Anal. At. Spectrom.* **2004**, *19*, 451–456. [CrossRef]
74. Legnaioli, S.; Lorenzetti, G.; Pardini, L.; Cavalcanti, G.H.; Palleschi, V. Applications of LIBS to the analysis of metals. In *Laser-Induced Breakdown Spectroscopy*; Musazzi, S., Perini, U., Eds.; Springer: Berlin/Heidelberg, Germany, 2014; Volume 182, pp. 169–193. [CrossRef]
75. Jochum, T.; Günther, J.U.; Bohling, C. Material analysis in fast industrial processes by LIBS: Technical and analytical solutions for inline process monitoring. *Photonics Views* **2019**, *16*, 56–59. [CrossRef]
76. Tognoni, E.; Palleschi, V.; Corsi, M.; Cristoforetti, G.; Omenetto, N.; Gornushkin, I.; Smith, B.W.; Winefordener, J.D. From sample to signal in laser-induced breakdown spectroscopy: A complex route to quantitative analysis. In *Laser-Induced Breakdown Spectroscopy (LIBS) Fundamentals and Applications*; Miziolek, A.W., Palleschi, V., Schechter, I., Eds.; Cambridge University Press: Cambridge, UK, 2006; pp. 122–170.
77. Russo, R.E.; Chan, W.-T.; Bryant, M.F.; Kinard, W.F. Laser ablation sampling with ICP-AES for the analysis of prototypic glasses. *J. Anal. At. Spectrom* **1995**, *10*, 295–301. [CrossRef]
78. Eppler, A.S.; Cremers, D.A.; Hickmott, D.D.; Ferris, M.J.; Koskelo, A.C. Matrix effects in the detection of Pb and Ba in soils using laser-induced breakdown spectroscopy. *Appl. Spectrosc.* **1996**, *50*, 1175–1181. [CrossRef]
79. Gornushkin, S.I.; Gornushkin, I.B.; Anzano, J.M.; Smith, B.W.; Winefordner, J.D. Effective normalization technique for correction of matrix effects in laser-induced breakdown spectroscopy detection of magnesium in powdered samples. *Appl. Spectrosc.* **2002**, *56*, 433–436. [CrossRef]
80. Lepore, K.H.; Fassett, C.I.; Breves, E.A.; Byrne, S.; Giguere, S.; Boucher, T.; Rhodes, J.M.; Vollinger, M.; Anderson, C.H.; Murray, R.W.; et al. Matrix effects in quantitative analysis of laser-induced breakdown spectroscopy (LIBS) of rock powders doped with Cr, Mn, Ni, Zn, and Co. *Appl. Spectrosc.* **2017**, *71*, 600–626. [CrossRef] [PubMed]
81. Sallé, B.; Lacour, J.L.; Mauchien, P.; Fichet, P.; Maurice, S.; Manhes, G. Comparative study of different methodologies for quantitative rock analysis by laser-induced breakdown spectroscopy in a simulated Martian atmosphere. *Spectrochim. Acta Part B* **2006**, *61*, 301–313. [CrossRef]
82. Rauschenbach, I.; Lazic, V.; Pavlov, S.G.; Hübers, H.W.; Jessberger, E.K. Laser induced breakdown spectroscopy on soils and rocks: Influence of the sample temperature, moisture and roughness. *Spectrochim. Acta Part B At. Spectrosc.* **2008**, *63*, 1205–1215. [CrossRef]
83. Cousin, A.; Sautter, V.; Fabre, C.; Maurice, S.; Wiens, R.C. Textural and modal analyses of picritic basalts with ChemCam laser-induced breakdown spectroscopy. *J. Geophys. Res. Planets* **2012**, *117*, E10. [CrossRef]
84. Diaz, D.; Hahn, D.W.; Molina, A. Evaluation of laser-induced breakdown spectroscopy (LIBS) as a measurement technique for evaluation of total elemental concentration in soils. *Appl. Spectrosc.* **2012**, *66*, 99–106. [CrossRef]
85. Harmon, R.S.; Russo, R.E.; Hark, R.R. Applications of laser-induced breakdown spectroscopy for geochemical and environmental analysis: A comprehensive review. *Spectrochim. Acta Part B At. Spectrosc.* **2013**, *87*, 11–26. [CrossRef]
86. Rapin, W.; Bousquet, B.; Lasue, J.; Meslin, P.Y.; Lacour, J.L.; Fabre, C.; Wiens, R.C.; Frydenvang, J.; Dehouck, E.; Maurice, S.; et al. Roughness effects on the hydrogen signal in laser-induced breakdown spectroscopy. *Spectrochim. Acta Part B At. Spectrosc.* **2017**, *137*, 13–22. [CrossRef]
87. Popov, A.M.; Zaytsev, S.M.; Seliverstova, I.V.; Zakuskin, A.S.; Labutin, T.A. Matrix effects on laser-induced plasma parameters for soils and ores. *Spectrochim. Acta Part B At. Spectrosc.* **2018**, *148*, 205–210. [CrossRef]

88. Xu, W.; Sun, C.; Tan, Y.; Gao, L.; Zhang, Y.; Yue, Z.; Shabbir, S.; Wu, M.; Zou, L.; Chen, F.; et al. Total alkali silica classification of rocks with LIBS: Influences of the chemical and physical matrix effects. *J. Anal. At. Spectrom.* **2020**, *35*, 1641–1653. [CrossRef]
89. Gorry, P.A. General least-squares smoothing and differentiation by the convolution (Savitzky-Golay) method. *Anal. Chem.* **1990**, *62*, 570–573. [CrossRef]
90. Wise, M.A. Trace element chemistry of lithium-rich micas from rare-element granitic pegmatites. *Miner. Pet.* **1995**, *55*, 203–215. [CrossRef]
91. Nironen, M. Central Finland Granitoid Complex—Explanation to a Map. In *Report of Investigation 157*; Geological Survey of Finland: Espoo, Finland, 2003; pp. 1–45. (Finnish with English Summary)
92. Chopin, F.; Korja, A.; Nikkilä, K.; Hölttä, P.; Korja, T.; Zaher, M.A.; Kurhila, M.; Eklund, O.; Rämö, O.T. The Vaasa Migmatitic Complex (Svecofennian Orogen, Finland): Buildup of a LP-HT Dome during Nuna Assembly. *Tectonics* **2020**, *39*, e2019TC005583. [CrossRef]
93. Brewer, E.O. *Soil Survey of Catawba County, North Carolina*; US Department of Agriculture, Soil Conservation Service: Washington, DC, USA, 1975; 47p.
94. Hashimoto, Y. Citrate sorption and biodegradation in acid soils with implications for aluminum rhizotoxicity. *Appl. Geochem.* **2007**, *22*, 2861–2871. [CrossRef]
95. Foster, M. Interpretation of the composition of lithium micas. *U.S. Geol. Survey Prof. Paper* **1960**, *354-E*, 115–147. [CrossRef]
96. Hawthorne, F.C.; Černý, P.; The Mica Group. *Short Course Handbook*; Mineralogical Association of Canada: Quebec City, QC, Canada, 1982; Volume 8, pp. 63–98.
97. Černý, P.; Burt, D. Paragenesis, crystallochemical characteristics, and geochemical evolution in micas in granite pegmatites. In *Micas*; Bailey, S.W., Ed.; Reviews in Mineralogy; Mineralogical Society of America: Washington, DC, USA, 1984; Volume 13, pp. 257–297. [CrossRef]
98. Rosales, G.D.; Pinna, E.G.; Suarez, D.S.; Rodriguez, M.H. Recovery Process of Li, Al and Si from Lepidolite by Leaching with HF. *Minerals* **2017**, *7*, 36. [CrossRef]
99. Xing, C.-M.; Wang, C.Y.; Wang, H. Magmatic-hydrothermal processes recorded by muscovite andcolumbite-group minerals from the Bailongshan rare-element pegmatites in the West Kunlun-Karakorum orogenic belt, NW China. *Lithos* **2020**, *364–365*, 105507. [CrossRef]
100. Llera, A.R.; Fuertes-Fuente, M.; Cepedal, A.; Martin-Izard, A. Barren and Li–Sn–Ta Mineralized pegmatites from NW Spain (Central Galicia): A comparative study of their mineralogy, geochemistry, and wallrock metasomatism. *Minerals* **2019**, *9*, 739. [CrossRef]
101. Roda-Robles, E.; Perez, A.P.; Roldan, F.V.; Fontan, F. The granitic pegmatites of the Fregeneda area (Salamanca, Spain): Characteristics and petrogenesis. *Miner. Mag.* **1999**, *63*, 535–558. [CrossRef]
102. Küster, D.; Romer, R.L.; Tolessa, D.; Zerihun, D.; Bheemalingeswara, K.; Melcher, F.; Oberthür, T. The Kenticha rare-element pegmatite, Ethiopia: Internal differentiation, U–Pb age and Ta mineralization. *Miner. Depos.* **2009**, *44*, 723–750. [CrossRef]
103. Deveaud, S.; Millot, R.; Villaros, A. The genesis of LCT-type granitic pegmatites, as illustrated by lithium isotopes in micas. *Chem. Geol.* **2015**, *411*, 97–111. [CrossRef]
104. Anderson, M.; Lentz, D.; McFarlane, C.; Falck, H. A geological, geochemical and textural study of an LCT pegmatite: Implications for the magmatic versus metasomatic origin of Nb-Ta mineralization in the Moose II pegmatite, Northwest Territories, Canada. *J. Geosci.* **2013**, *58*, 299–320. [CrossRef]
105. Van Lichtervelde, M.; Grégoire, M.; Linnen, R.L.; Béziat, D.; Salvi, S. Trace element geochemistry by laser ablation ICP-MS of micas associated with Ta mineralization in the Tanco pegmatite, Manitoba, Canada. *Contrib. Miner. Petrol.* **2008**, *155*, 791–806. [CrossRef]
106. Martins, T.; Linnen, R.L.; Fedikow, M.A.F.; Singh, J. Whole-rock and mineral geochemistry as exploration tools for rare-element pegmatite in Manitoba: Examples from the Cat Lake–Winnipeg River and Wekusko Lake pegmatite fields (parts of NTS 52L6, 63J13). *Manit. Geol. Survey Rep. Act.* **2017**, 42–51.
107. Grant, K.J.; Paul, G.L.; O'Neill, J.A. Quantitative elemental analysis of iron ore by laser-induced breakdown spectroscopy. *Appl. Spectrosc.* **1991**, *45*, 701–705. [CrossRef]
108. Death, D.; Cunningham, A.; Pollard, L. Multi-element analysis of iron ore pellets by laser-induced breakdown spectroscopy and principal components regression. *Spectrochim. Acta Part B At. Spectrosc.* **2008**, *63*, 763–769. [CrossRef]
109. Yaroshchyk, P.; Death, D.L.; Spencer, S.J. Comparison of principal components regression, partial least squares regression, multi-block partial least squares regression, and serial partial least squares regression algorithms for the analysis of Fe in iron ore using LIBS. *J. Anal. At. Spectrom.* **2011**, *27*, 92–98. [CrossRef]
110. Klus, J.; Mikysek, P.; Prochazka, D.; Pořízka, P.; Prochazková, P.; Novotny, J.; Trojek, T.; Novotný, K.; Slobodník, M.; Kaiser, J. Multivariate approach to the chemical mapping of uranium in sandstone-hosted uranium ores analyzed using double pulse Laser-Induced Breakdown Spectroscopy. *Spectrochim. Acta Part B At. Spectrosc.* **2016**, *123*, 143–149. [CrossRef]
111. Álvarez, J.; Velásquez, M.; Myakalwar, A.K.; Sandoval, C.; Fuentes, R.; Castillo, R.; Sbarbaro, D.; Yáñez, J. Determination of copper-based mineral species by laser induced breakdown spectroscopy and chemometric methods. *J. Anal. At. Spectrom.* **2019**, *34*, 2459–2468. [CrossRef]
112. Rosenwasser, S.; Asimellis, G.; Bromley, B.; Hazlett, R.; Martin, J.; Pearce, T.; Zigler, A. Development of a method for automated quantitative analysis of ores using LIBS. *Spectrochim. Acta Part B At. Spectrosc.* **2001**, *56*, 707–714. [CrossRef]

113. Gaft, M.; Sapir-Sofer, I.; Modiano, H.; Stana, R. Laser induced breakdown spectroscopy for bulk minerals online analyses. *Spectrochim. Acta Part B At. Spectrosc.* **2007**, *62*, 1496–1503. [CrossRef]
114. Cheng, X.; Yang, X.; Zhu, Z.; Guo, L.; Li, X.; Lu, Y.; Zeng, X. On-stream analysis of iron ore slurry using laser-induced breakdown spectroscopy. *Appl. Opt.* **2017**, *56*, 9144–9149. [CrossRef] [PubMed]
115. Khajehzadeh, N.; Haavisto, O.; Koresaar, L. On-stream mineral identification of tailing slurries of an iron ore concentrator using data fusion of LIBS, reflectance spectroscopy and XRF measurement techniques. *Miner. Eng.* **2017**, *113*, 83–94. [CrossRef]
116. Rifai, K.; Doucet, F.; Özcan, L.; Vidal, F. LIBS core imaging at kHz speed: Paving the way for real-time geochemical applications. *Spectrochim. Acta Part B At. Spectrosc.* **2018**, *150*, 43–48. [CrossRef]
117. Foucaud, Y.; Fabre, C.; Demeusy, B.; Filippova, I.; Filippov, L. Optimisation of fast quantification of fluorine content using handheld laser induced breakdown spectroscopy. *Spectrochim. Acta Part B At. Spectrosc.* **2019**, *158*, 105628. [CrossRef]